Direct recruitment of Mis18 to interphase spindle pole bodies promotes CENP-A chromatin assembly

Article

Current Biology

Direct recruitment of Mis18 to interphase spindle pole bodies promotes CENP-A chromatin assembly

Highlights

- Mis18 directly associates with the spindle pole body (SPB) protein Sad1
- Mis18C components are spatially sequestered to SPBs independently of centromeres
- Efficient CENP-A^{Cnp1} chromatin establishment requires Mis18-Sad1 association
- Sad1 acts in parallel with CENP-C^{Cnp3} to maintain CENP-A^{Cnp1} at centromeres

Authors

Nitobe London, Bethan Medina-Pritchard, Christos Spanos, Juri Rappsilber, A. Arockia Jeyaprakash, Robin C. Allshire

Correspondence

robin.allshire@ed.ac.uk

In brief

London et al. unexpectedly identify Sad1, a key spindle pole body linker of nucleoskeleton and cytoskeleton (LINC) component, as a non-centromeric receptor for the Mis18 complex CENP-A^{Cnp1} assembly factors. Mis18C-Sad1 association contributes to both the establishment and maintenance of CENP-A^{Cnp1} chromatin at centromeres.

London et al., 2023, Current Biology *33*, 4187–4201
October 9, 2023
https://doi.org/10.1016/j.cub.2023.08.063

CellPress

Current Biology

CellPress
OPEN ACCESS

Article

Direct recruitment of Mis18 to interphase spindle pole bodies promotes CENP-A chromatin assembly

Nitobe London,[1] Bethan Medina-Pritchard,[1] Christos Spanos,[1] Juri Rappsilber,[1,2] A. Arockia Jeyaprakash,[1,3] and Robin C. Allshire[1,4,5,*]

[1]Wellcome Trust Centre for Cell Biology, Institute of Cell Biology, School of Biological Sciences, The University of Edinburgh, Edinburgh EH9 3BF, Scotland, UK

[2]Institute of Biotechnology, Technische Universität, 13355 Berlin, Germany

[3]Gene Center and Department of Biochemistry, Ludwig-Maximilians-Universität München, 81377 Munich, Germany

[4]X (formerly Twitter): @Allshire_Lab

[5]Lead contact

*Correspondence: robin.allshire@ed.ac.uk

https://doi.org/10.1016/j.cub.2023.08.063

SUMMARY

CENP-A chromatin specifies mammalian centromere identity, and its chaperone HJURP replenishes CENP-A when recruited by the Mis18 complex (Mis18C) via M18BP1/KNL2 to CENP-C at kinetochores during interphase. However, the Mis18C recruitment mechanism remains unresolved in species lacking M18BP1, such as fission yeast. Fission yeast centromeres cluster at G2 spindle pole bodies (SPBs) when CENP-A^{Cnp1} is replenished and where Mis18C also localizes. We show that SPBs play an unexpected role in concentrating Mis18C near centromeres through the recruitment of Mis18 by direct binding to the major SPB linker of nucleoskeleton and cytoskeleton (LINC) component Sad1. Mis18C recruitment by Sad1 is important for CENP-A^{Cnp1} chromatin establishment and acts in parallel with a CENP-C-mediated Mis18C recruitment pathway to maintain centromeric CENP-A^{Cnp1} but operates independently of Sad1-mediated centromere clustering. SPBs therefore provide a non-chromosomal scaffold for both Mis18C recruitment and centromere clustering during G2. This centromere-independent Mis18-SPB recruitment provides a mechanism that governs *de novo* CENP-A^{Cnp1} chromatin assembly by the proximity of appropriate sequences to SPBs and highlights how nuclear spatial organization influences centromere identity.

INTRODUCTION

Centromeres are chromosomal sites that mediate accurate chromosome segregation during cell division. Many questions remain with respect to determining how centromeres are specified and maintained at a single location on monocentric chromosomes. Chromatin containing the centromere-specific histone H3 variant CENP-A (Cnp1 in the fission yeast, *Schizosaccharomyces pombe*) underlies kinetochores at many eukaryotic centromeres including those of human chromosomes. Epigenetic mechanisms maintain centromeres by templating CENP-A deposition at sites where CENP-A chromatin was previously assembled.[1,2] However, *de novo* centromere formation at chromosomal locations lacking CENP-A can also occur.[3–7] Such neocentromere formation may contribute to speciation and oncogenesis.[8–11] Quality control mechanisms hinder neocentromere formation by promoting removal of CENP-A from non-centromeric locations.[12–14] Multiple mechanisms therefore ensure centromere maintenance at their correct locations to promote cell viability.

Maintenance of centromere location is ultimately determined by CENP-A chromatin assembly factor activity. In many species, including *S. pombe*, centromeres are composed of central core domains of high CENP-A^{Cnp1} density flanked by repetitive DNA sequences that form heterochromatin.[9] Centromeres are frequently formed on AT-rich DNA, but underlying sequence alone is generally insufficient to specify centromere formation except for point centromeres such as those of budding yeast.[9] During replication, CENP-A nucleosomes are distributed to both sister chromatids, halving CENP-A levels at centromeres, with histone H3 nucleosomes initially assembled as placeholders.[15] CENP-A^{Cnp1} nucleosomes replace H3 nucleosomes via the activity of the histone chaperone HJURP (*S. pombe* Scm3) and associated factors during G2 in *S. pombe* and telophase/G1 in human cells.[16–20] Centromere-specific recruitment of HJURP^{Scm3} is mediated by the Mis18 complex (Mis18C), which is composed of Mis18, Mis16, Eic1/Mis19, and Eic2/Mis20 in *S. pombe*[21–24] and hMis18α, hMis18β, and Mis18BP1/KNL2 (M18BP1) in human cells.[25–27] *S. pombe* Mis18 is homologous to both hMis18α and hMis18β, and *S. pombe* Mis16 is equivalent to human RbAp46/48.[21,25] M18BP1 binds CENP-A, CENP-I, and CENP-C at metazoan kinetochores and consequently recruits Mis18C to centromeres.[28–30] However, *S. pombe* lacks a M18BP1 ortholog, and although *S. pombe* Mis18 directly interacts with CENP-C^{Cnp3} *in vitro*, mutations in Mis18 that disrupt CENP-C^{Cnp3}-Mis18 association only modestly reduce CENP-A^{Cnp1} localization at centromeres.[24,25,31] Furthermore, *S. pombe* CENP-C^{Cnp3} is not

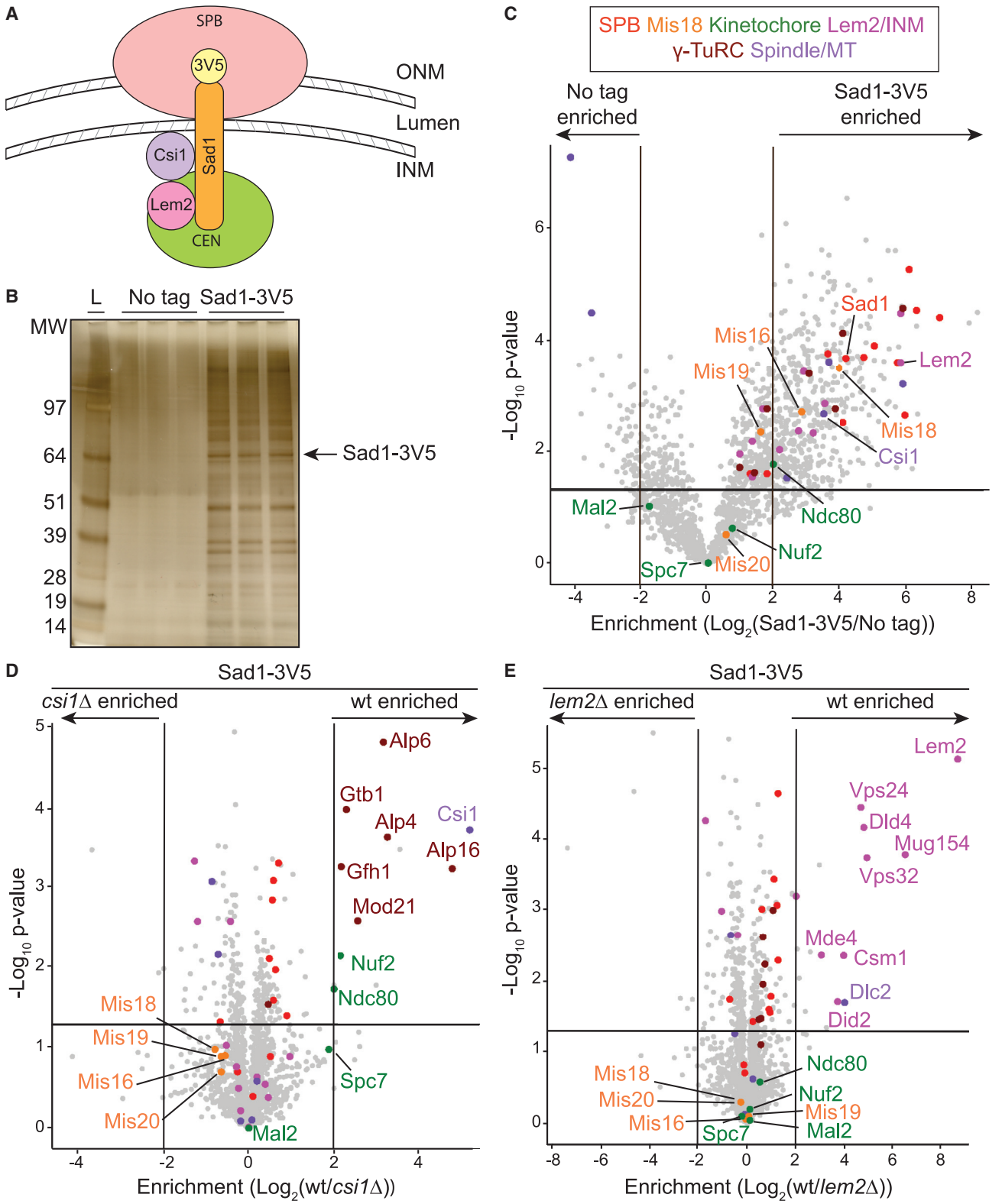

Figure 1. Centromere-, INM-, and spindle-related proteins copurify with Sad1

(A) Diagram of interphase *S. pombe* spindle pole body (SPB) association with the nuclear membrane, showing Sad1 localization at the inner nuclear membrane (INM), its association with centromeres, and its interaction with Csi1 and Lem2. Centromeres of all three chromosomes cluster at SPBs. ONM, outer nuclear membrane.

(legend continued on next page)

essential, indicating that other Mis18C recruitment mechanisms remain to be discovered.[32]

All centromeres associate with the nuclear periphery in a cluster adjacent to the spindle pole body (SPB) in yeasts, and centromere clustering during interphase is widespread in eukaryotic cells including those of human tissues.[10,33–35] SPBs are the yeast nuclear mitotic microtubule organizing centers—equivalent to metazoan centrosomes.[36] Centromeres and thus kinetochore proteins localize close to SPBs in G2 *S. pombe* cells. SPB-centromere clustering ensures efficient kinetochore microtubule capture in early mitosis and also promotes efficient CENP-A^{Cnp1} deposition on centromeric DNA.[37–41] Notably, CENP-A^{Cnp1} incorporation depends on spatial proximity of substrate DNA to SPB-centromere clusters.[41] This is consistent with the concentration of Mis18C and HJURP^{Scm3} with clustered centromeres throughout G2, when new CENP-A^{Cnp1} deposition occurs.[18,21,22,24,42,43] Compromised Mis18C function results in loss of both CENP-A^{Cnp1} and HJURP^{Scm3} from *S. pombe* centromeres, but Mis18 remains localized when CENP-A^{Cnp1}, HJURP^{Scm3}, or CENP-C^{Cnp3} function is disrupted.[21,31,42,43] Mis18C components may therefore localize to SPB-centromere clusters independently of centromere proteins.

It remains unclear how SPB-centromere association is mediated. Most *S. pombe* SPB proteins reside on the cytoplasmic plaque on the outer nuclear membrane during interphase, whereas only a few reside on the inner nuclear membrane (INM)[36] (Figure 1A). Known INM-associated proteins at SPBs include gamma-tubulin ring complex (γ-TuRC) components, the INM-associated proteins Lem2 and Nur1/Mug154, the spindle- and kinetochore-linking protein Csi1, and the linker of nucleoskeleton and cytoskeleton (LINC) complex protein Sad1.[38,44–47] G2 SPB-centromere clustering is moderately disrupted in cells lacking Csi1 and is exacerbated by loss of Lem2.[38,48,49] Sad1 links centromeres to the nuclear periphery, and a proportion of *sad1* mutant cells completely dissociate all centromeres from SPBs.[50,51] Defective kinetochore function perturbs SPB-centromere association, suggesting that Sad1 or Csi1 may interact directly with kinetochore proteins to mediate SPB-centromere connections.[38,52,53] Although SPB-centromere linkages depend on Sad1, the protein interaction network at the INM remains poorly understood.

To better characterize *S. pombe* SPB-centromere association, we adopted an *in vivo* cleavage approach to identify proteins that specifically associate with the nucleoplasmic region of Sad1. This strategy, along with biochemical and structural analyses, revealed that Mis18 directly interacts with the first 60 residues of Sad1. Our separation-of-function *sad1-4A* mutant causes Mis18C, but not centromeres, to dissociate from SPBs. This mutant revealed that recruitment of Mis18C by Sad1 to SPBs promotes *de novo* CENP-A^{Cnp1} chromatin establishment on naive centromere DNA and contributes to endogenous CENP-A^{Cnp1} chromatin maintenance. Our analyses show that this Mis18-Sad1 recruitment pathway at SPBs also operates in parallel to a centromere-based Mis18 recruitment pathway to maintain existing centromeres. Thus, we uncover a novel mechanism for Mis18C recruitment that does not require direct recruitment of Mis18C to kinetochores for CENP-A deposition at centromeres. Rather, Mis18C operates through a SPB-based platform distinct from kinetochores and even chromosomes, highlighting the importance of the spatial positioning of centromeres within nuclei for centromere identity and integrity.

RESULTS

SPB, INM, and kinetochore proteins associate with Sad1

The connection of interphase SPBs with centromeres depends on Sad1, but the full set of proteins that reside on the nucleoplasmic face of SPBs with Sad1 is not known (Figure 1A). To identify Sad1-associated proteins, immunoprecipitated (IP) Sad1-3V5 (C-terminally 3xV5-tagged) from cell extracts was analyzed by SDS-PAGE and label-free quantitative mass spectrometry (IP/LFQ-MS) and compared with untagged control cell IPs (Figures 1B and 1C). A complete set of structural SPB proteins, components of the INM, γ-TuRC, kinetochore proteins, the Mis18C, and spindle-associated proteins were enriched with Sad1-3V5 (Figure 1C; Table S1; Data S1A).

Csi1 and Lem2 associate with Sad1 and contribute to centromere clustering at SPBs.[38,48] We next identified proteins that show reduced Sad1-3V5 association in cells lacking Csi1, Lem2, or both. Enrichment of γ-TuRC and kinetochore proteins (Nuf2 and Ndc80) with Sad1-3V5 was reduced in *csi1Δ* cells (Figure 1D; Data S1B), whereas levels of ESCRT proteins, dynein light chain, monopolin proteins, and the Lem2-binding protein Nur1/Mug154 were reduced in *lem2Δ* cells (Figure 1E; Data S1C). Both sets of proteins also showed specific reduction in their association with Sad1-3V5 in *csi1Δlem2Δ* cells, with essentially no loss of additional proteins (Figure S1A; Data S1D). These findings are consistent with the known functions of Csi1 in promoting spindle formation and centromere clustering[38,54] and the role of Lem2 in nuclear membrane remodeling.[55–57] Although Csi1 clearly mediates association of some kinetochore proteins with Sad1-3V5, enrichment of Mis18C components was unaffected by Csi1 and/or Lem2 loss, suggesting that Mis18C may associate with Sad1-3V5 by a distinct route (Figures 1D, 1E, S1A, and S1B).

Inducible TEV-mediated cleavage reveals that Mis18 association with SPBs depends on the Sad1 N-terminal region

The domain organization of Sad1 indicates that only the first N-terminal 167 residues (before the transmembrane domain) protrude into the nucleoplasm (Figure 2A). Additionally, the temperature-sensitive *sad1-2* mutation (T3S and S52P) causes centromeres to detach from interphase SPBs.[51] SPB-centromere

(B) Silver stained SDS-PAGE gel of three independent anti-V5 IPs from extracts of untagged or *sad1-3V5* cells used for LFQ-MS. L, MW ladder, kDa.
(C) Volcano plot of LFQ-MS data comparing proteins enriched in anti-V5 Sad1-3V5 IPs relative to untagged control IPs. Lower cutoff corresponds to p = 0.05 and threshold bars are placed at $\log_2(2)$ (equal to 4-fold enrichment). Samples compared by Student's t test with alpha = 0.05 (see STAR Methods).
(D and E) Volcano plots of LFQ-MS data comparing proteins enriched with Sad1-3V5 in *csi1Δ* or *lem2Δ* cells relative to wild-type (WT) cells. Volcano plot protein category components are listed in Table S1 and color coded as indicated.
See also Figure S1 and Data S1A–S1C.

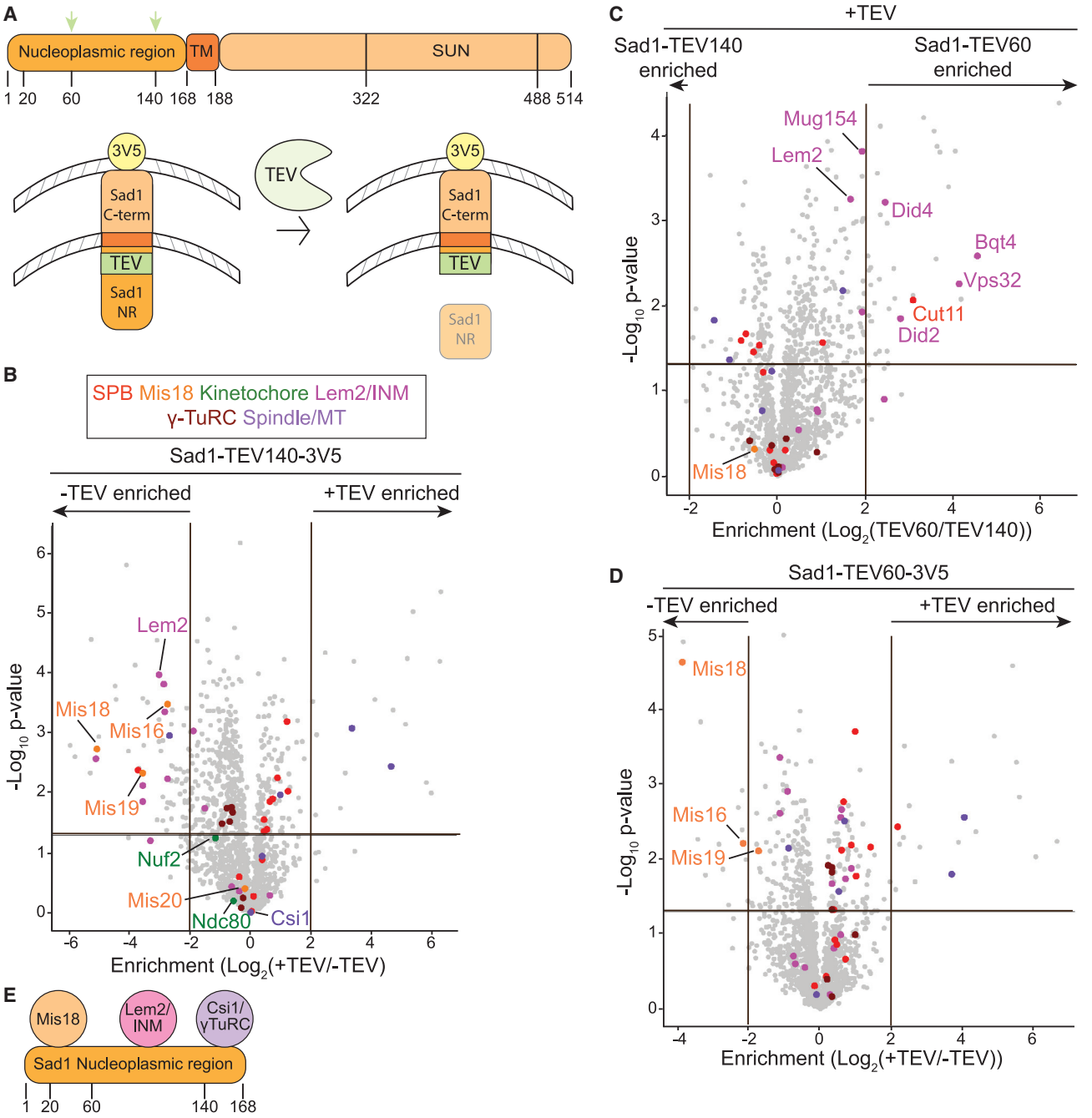

Figure 2. *In vivo* TEV cleavage of the Sad1 N terminus disrupts Mis18C association with Sad1

(A) Diagram showing Sad1 protein domains and Sad1-TEV cleavage strategy. Top: Sad1 TEV sites were inserted at residues 60 or 140 (green arrows) in the nucleoplasmic region of Sad1. Numbering indicates Sad1 amino acid positions. TM, transmembrane domain; SUN, Sad1/UNC84 lumenal domain. Bottom: thiamine washout induces nuclear-targeted TEV protease expression (NLS-9myc-TEV-2xNLS), cleaving Sad1 at an inserted TEV recognition site (green). NR, nucleoplasmic region.

(B) Volcano plot of LFQ-MS data comparing proteins enriched in anti-V5 Sad1-TEV140-3V5 IPs before (–) or after (+) TEV cleavage.

(C) Volcano plot of LFQ-MS data comparing proteins enriched in anti-V5 Sad1-TEV60-3V5 and Sad1-TEV140-3V5 IPs after TEV cleavage.

(D) Volcano plot of LFQ-MS data comparing proteins enriched in anti-V5 Sad1-TEV60-3V5 IPs before (–) or after (+) TEV cleavage.

(E) Cartoon summarizing Mis18C-, Lem2/INM-, and Csi1/γ-TuRC-interacting regions within the nucleoplasmic region of Sad1 based on LFQ-MS data ± TEV cleavage. Volcano plot protein category components are listed in Table S1 and color coded as indicated.

See also Figure S2 and Data S2B–S2D.

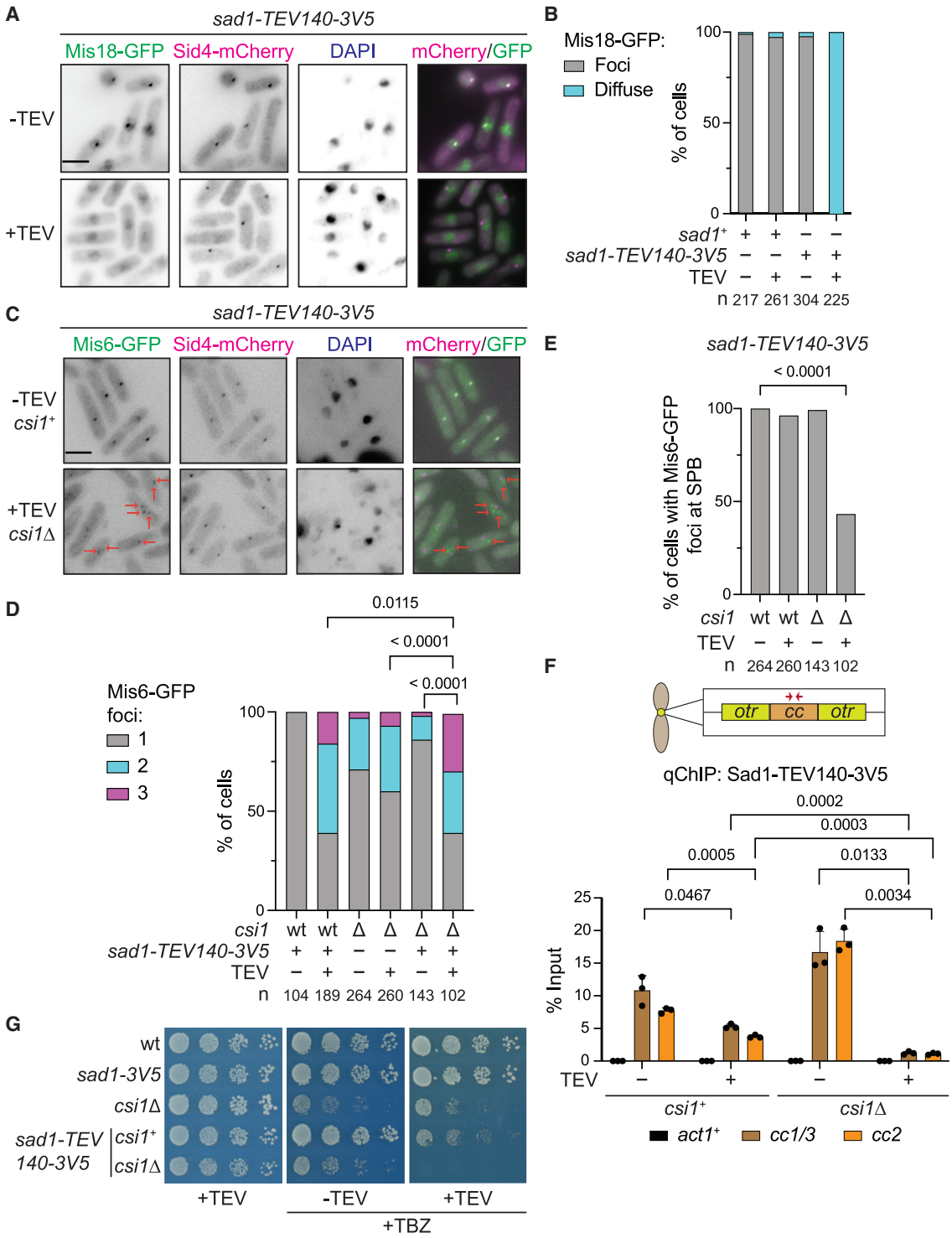

Figure 3. TEV cleavage in the Sad1 nucleoplasmic region dissociates Mis18 and kinetochores from SPBs *in vivo*

(A) Localization of Mis18-GFP and the SPB protein Sid4-mCherry in *sad1-TEV140-3V5* cells with (+) or without (–) TEV expression induced for 16 h from *pnmt1-TEV*.

(B) Quantification of cells (%, cell number n below) with normal Mis18-GFP focus or diffuse signal.

(C) Example localization of Mis6-GFP and SPB protein Sid4-mCherry in *sad1-TEV140-3V5* cells with (+) or without (–) TEV expression in the presence (*csi1*$^{+}$) or absence (*csi1Δ*) of *csi1*. Arrows indicate Mis6-GFP spots separated from the SPB.

(D) Quantification of cells (%, cell number n below) with 1, 2, or 3 separate Mis6-GFP foci. *sad1-TEV140-3V5* cells (+) or wild-type *sad1*$^{+}$ (–) were grown with (+) or without (–) TEV expression in the presence or absence of *csi1* (WT or Δ, respectively). p values calculated by χ^2 test.

(legend continued on next page)

clustering therefore relies on this N-terminal region. To selectively and inducibly disrupt this region, we inserted a tobacco etch virus (TEV) protease cleavage site at amino acid positions 60 or 140 in the 3V5-tagged endogenous *sad1*$^{+}$ gene to cleave Sad1-3V5 protein at these positions upon TEV protease expression (Figure 2A). Nuclear-targeted TEV protease expression cleaved approximately 80% of Sad1-TEV140-3V5 in cells (Figures S2A and S2B). Immunolocalization showed that the C-terminal portion of cleaved Sad1-TEV140-3V5 remained colocalized with a SPB marker (Figure S2C). TEV expression rendered *sad1-TEV140-3V5* cells mildly thiabendazole- (TBZ) and temperature-sensitive compared with control cells, reflecting defective centromere, kinetochore, or spindle function. As expected, this sensitivity depended on TEV expression and the presence of TEV sites (Figures S2D and S2E). The N-terminal product of Sad1-TEV140-3V5 cleavage was presumably degraded as it was undetectable when the 3V5 tag was fused to the N terminus of Sad1 (3V5-Sad1-TEV140, Figure S2F). We therefore only analyzed the stable C-terminal part of Sad1-3V5 in subsequent cleavage experiments. This system allows inducible *in vivo* cleavage of the Sad1 N terminus and disruption of Sad1 function.

To identify proteins that specifically associate with the Sad1 N-terminal region, we compared sets of proteins associated with uncleaved and cleaved Sad1-TEV140-3V5 by IP/LFQ-MS analysis. Comparison of uncleaved Sad1-TEV140-3V5 and Sad1-3V5 showed that copurifying proteins were largely unaffected by TEV site insertion (Figure S2G; Data S2A). Proteins depleted from Sad1-TEV140-3V5 purifications upon its cleavage include Lem2, Lem2-dependent proteins (see Figure 1E), and Mis18C components (Figure 2B; Data S2B). In contrast, levels of Csi1 and Csi1-dependent proteins were unaffected (Figure 2B; Data S2B; see Figure 1D), suggesting that they associate with Sad1 through residues 140–167, which remain between the cleavage site and the transmembrane region.

To locate more precisely which parts of the Sad1 N-terminal region recruit specific proteins, we compared protein enrichments in Sad1-TEV60-3V5 and Sad1-TEV140-3V5 purifications. Lem2 and associated proteins were retained following Sad1-TEV60-3V5 cleavage, suggesting that Lem2 associates with Sad1 mainly through residues 60–140 (Figure 2C; Data S2C). In contrast, Mis18C components were lost following TEV cleavage at position 60, indicating that they are recruited by the N-terminal 60 residues of Sad1 and independently of Lem2 (Figure 2D; Data S2D). These results demonstrate that specific sets of proteins tend to associate with particular regions of Sad1 (Figure 2E).

We next examined the *in vivo* impact of Sad1 cleavage on the localization of SPB/centromere proteins in cells expressing Sad1-TEV140-3V5. In agreement with LFQ-MS analysis, cleavage delocalized Mis18-GFP from SPB-centromere clusters and diminished Lem2-GFP SPB-associated signals, whereas Csi1-GFP was clearly still visible as a focus despite slightly lower SPB-normalized intensities (Figures 3A, 3B, and S3A–S3C). Thus, Mis18C and the SPB proteins Lem2 and Csi1 associate with Sad1 through distinct subregions of the Sad1 N-terminal region *in vivo*.

SPB-centromere clustering involves multiple interactions via the Sad1 N-terminal region

Sad1 cleavage enabled us to dissect how centromeres associate with SPBs. The Mis6-GFP kinetochore protein marks centromere location and thereby indicates the integrity of SPB-centromere clustering. All three centromeres cluster, producing a single Mis6-GFP signal at G2 SPBs, as quantified in wild-type (WT) cells expressing uncleaved Sad1-TEV140-3V5 (Figures 3C, 3D, and S3D). Cleavage of Sad1-TEV140-3V5 dramatically disrupted SPB-centromere clustering with many cells displaying two or three distinct Mis6-GFP foci (Figures 3C, 3D, and S3D), similar to cells lacking Csi1.[38] However, as the association of Csi1 with Sad1 remains intact upon Sad1-TEV140-3V5 cleavage (Figure 2B), the declustering phenotype suggested that the Sad1 N-terminal region contributes to the following two mechanisms of SPB clustering: one operating through residues 1–140 and the other via Csi1 association with residues 140–167 that remain after TEV cleavage. To test this possibility, we quantified the number of separate Mis6-GFP centromere foci in WT and *csi1Δ* cells with and without Sad1-TEV140-3V5 cleavage. The proportion of cells with three Mis6-GFP foci (declustered centromeres) upon Sad1-TEV140-3V5 cleavage was greater in *csi1Δ* than *csi1*$^{+}$ cells and increased relative to *csi1*Δ cells with intact Sad1 (Figure 3D). Strikingly, almost half of *csi1Δ* cells with cleaved Sad1-TEV140-3V5 showed complete dissociation of all Mis6-GFP marked centromeres from SPBs, an arrangement not observed in cells with only Sad1-TEV140-3V5 cleaved or just lacking Csi1 (Figures 3C, 3E, and S3D).

As a distinct approach to determine the impact of Sad1-TEV140-3V5 cleavage, we assessed SPB-centromere association using quantitative chromatin immunoprecipitation (qChIP). Sad1 is enriched over the central domain of *S. pombe* centromeres.[38] We found that Sad1-TEV140-3V5 cleavage significantly reduced Sad1 enrichment on centromere DNA when combined with *csi1*Δ (Figure 3F). The increase in TBZ sensitivity of *csi1*Δ and *bub1Δ* cells detected when combined with Sad1-TEV140-3V5 cleavage is also consistent with SPB-centromere clustering contributing to kinetochore function during mitosis (Figures 3G and S3E). We conclude that SPB-centromere association via the Sad1 nucleoplasmic region is mediated by two pathways, only one of which requires Csi1 function.

(E) Quantification of cells (%, cell number n below) retaining a Mis6-GFP focus at SPBs in wild-type (WT) and *csi1Δ* cells with (+) or without (–) Sad1-TEV140-3V5 cleavage. p value calculated by χ^2 test.
(F) Anti-V5 ChIP-qPCR for Sad1-TEV140-3V5 on central core domains of centromeres (*cc1/3* and *cc2*, red arrows) and the control *act1* locus (actin) in wild-type and *csi1*Δ cells with (+) or without (–) Sad1-TEV140-3V5 cleavage. Error bars are SD. p values calculated with Welch's t test. n = 3 biological replicates for each condition.
(G) Serial dilution growth assays of wild-type *csi1*$^{+}$ and *csi1Δ* cells on plates with (+) or without (–) TEV expression in the presence or absence of TBZ at 10 μg/mL. Wild-type (WT), *sad1-3V5* and *csi1*Δ cells included as controls for TBZ sensitivity.
See also Figure S3.

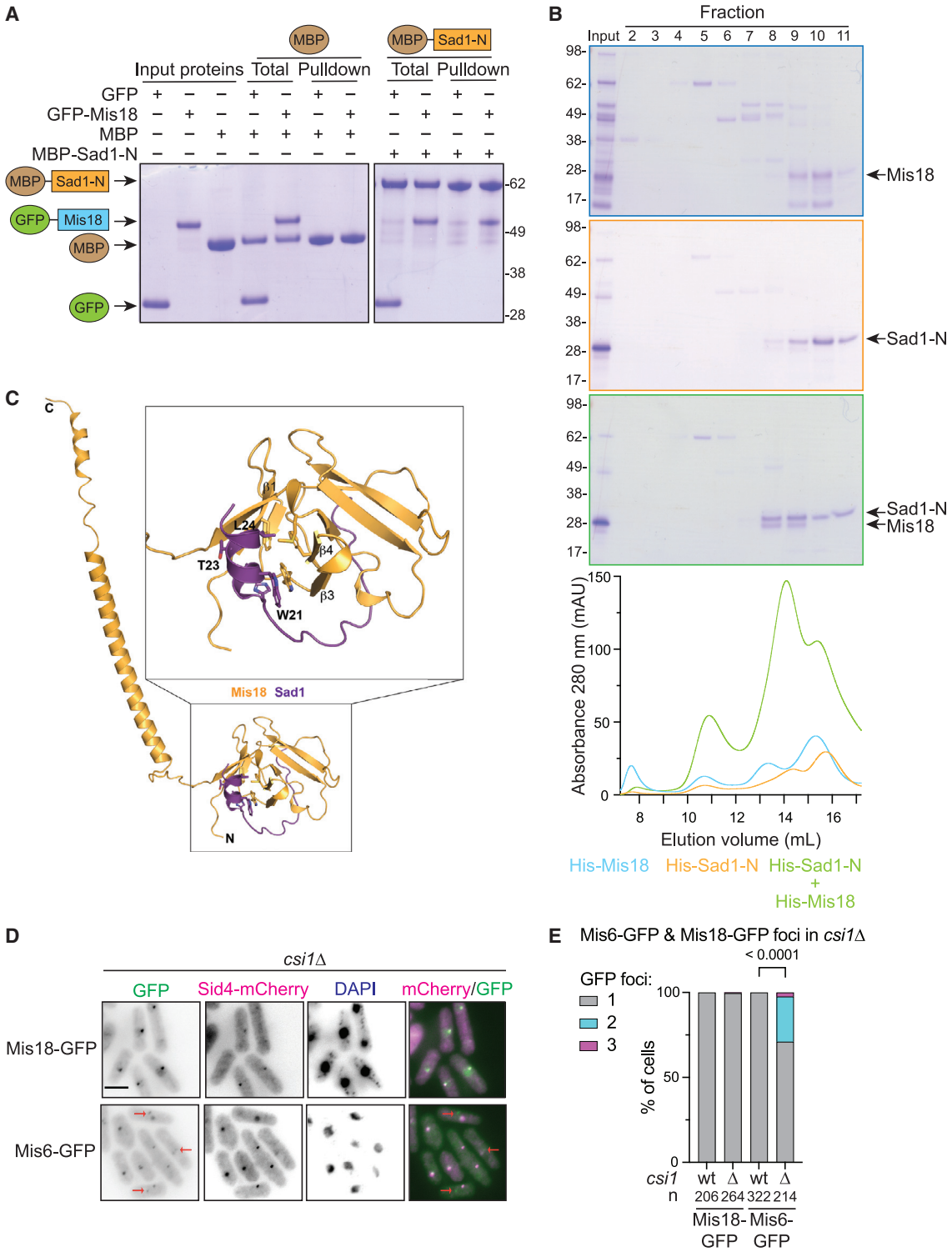

Figure 4. Mis18 directly binds the N-terminal region of Sad1 *in vitro*

(A) *In vitro* binding assays for recombinant GFP-Mis18 full length or GFP (control) to MBP-Sad1-N (residues 2–167, nucleoplasmic region) or MBP bound to amylose resin. Size markers: kDa.

(B) His-tagged full-length Mis18 and Sad1-N (nucleoplasmic region, 2–167) proteins were expressed individually or coexpressed, affinity purified, and fractionated on a Superdex 200 10/300 GL column. Elution profiles for each protein alone or coexpressed shown below. Size markers: kDa.

(C) Mis18 residues 1–194 and Sad1 residues 1–167 were modeled using Colabfold Alphafold2 notebook.[58] Visualization and analysis of interactions were performed using PyMOL.

(legend continued on next page)

Purified Sad1 nucleoplasmic region directly binds Mis18

Mis18 appeared to associate with Sad1 independently of centromeres, suggesting that Mis18 may interact directly with Sad1. *In vitro* binding assays with recombinant proteins showed that MBP-Sad1-N (residues 2–167) can bind to GFP-Mis18, but not GFP alone (Figure 4A). In addition, His-Sad1-N and His-Mis18 coexpressed in *E. coli* co-eluted at a lower volume than either protein alone in size-exclusion chromatography, indicating that they form a complex (Figure 4B). Thus, the Sad1 nucleoplasmic region exhibits robust direct binding with Mis18.

Similar *in vitro* binding assays were used to further dissect which regions of Mis18 mediate Sad1-N binding. Neither the N-terminal Yippee domain of Mis18 (residues 1–120) nor the α-helical C-terminal region (121–194) alone exhibited MBP-Sad1-N binding (Figure S4A). Furthermore, removal of the basically charged C-terminal tail (ct) from Mis18 (residues 169–194, $Mis18_{1–168}$/Mis18Δct)[59] prevented its association with MBP-Sad1-N (Figure S4B). *S. pombe* cells expressing only Mis18Δct are viable, but temperature sensitive, indicating that Mis18 function is compromised (Figure S4C). Moreover, co-immunoprecipitation (coIP) assays showed that the *in vivo* association of Sad1-3FLAG with Mis18Δct-3V5 was reduced relative to that of full-length Mis18-3V5 (Figure S4D).

To gain structural insights into the mode of Sad1 binding to Mis18, we generated an Alphafold model. Our high-confidence model predicts direct interaction between a short Sad1 helical segment spanning amino acid residues 18–25 with a hydrophobic pocket formed by the Mis18 Yippee domain (Figure 4C). Although the N-terminal region of Mis18 containing this pocket did not bind MBP-Sad1-N *in vitro* (Figure S4A), we found that this helical region of Sad1 was required for Mis18 association *in vivo* (see the next section and discussion). Interestingly, the equivalent surface of human Mis18α has been implicated in M18BP1 binding and was shown to be critical for centromere recruitment of human Mis18C.[30]

Sad1 recruits Mis18 to SPBs independently of centromeres

The *in vitro* binding assays and the difference between Mis18-GFP and Mis6-GFP localization in cells with cleaved Sad1-TEV140-3V5 (diffuse vs. foci, respectively, Figures 3A–3C) suggest that in *S. pombe*, Mis18 is recruited to SPB-centromere clusters primarily via SPBs, rather than via centromeres or constitutively associated kinetochore proteins. This conclusion is supported by our finding that Mis18-GFP localization was unaffected in *csi1Δ* cells, whereas Mis6-GFP centromere signals were frequently detected away from SPBs (Figures 4D, 4E, and S4E). Thus, Mis18 G2 localization appears to be mainly driven by its direct association with Sad1 at SPBs, not centromeres.

To determine if centromere clustering with SPBs depends on the association of Sad1 with Mis18, we sought conditions that more precisely disrupt Mis18 recruitment to SPBs. The N-terminal 60 Sad1 residues mediate Mis18C binding (Figures 2B–2E), and our structural analysis predicted that Sad1 interacts with Mis18 through the short α-helical 21-WSTL-24 region (Figures 4C and S5A). We therefore replaced WSTL with four alanine residues, generating the *sad1-4A* mutation at the endogenous *sad1* locus. *sad1-4A* did not significantly affect Sad1 protein levels, localization, or growth under standard conditions (Figures 5A and S5B–S5D). However, the localization of Mis18-GFP and the Mis18C component Eic1/Mis19-GFP at SPBs was disrupted in *sad1-4A* cells, giving diffuse signals similar to that of Mis18-GFP upon Sad1-TEV140-3V5 cleavage (Figures 5B and S5E). In contrast, Mis6-GFP-marked centromeres and the CENP-A^{Cnp1} chaperone $HJURP^{Scm3}$ remained localized close to SPBs in *sad1-4A* cells (Figures 5B and S5F). Furthermore, *sad1-4A* disrupted Mis18-3FLAG coIP with Sad1-3V5 (Figure S5G). Thus, mutation of four residues close to the Sad1 N terminus disrupts association of Mis18, but not centromeres, with SPBs.

To assess the specificity of *sad1-4A* for disrupting the Mis18-Sad1 interaction, we compared proteins enriched in Sad1-3V5 and Sad1-4A-3V5 IPs. LFQ-MS analyses showed that mainly Mis18C components were depleted in Sad1-4A-3V5 purifications (Figure 5C; Data S3A and S3B). Apart from Mis18C, four other proteins exhibited reduced association with Sad1-4A-3V5 (Ima1, Mak3, Mas2, and Qcr1; Data S3A). As Mas2 and Qcr1 are mitochondrial proteins and Mak3 is a cytoplasmic kinase, these presumably represent purification artifacts. Enrichment of the nuclear envelope protein Ima1 was only marginally affected, and Ima1 has no reported connection with Mis18C or centromere proteins.[60] In addition, qChIP revealed that enrichment of Mis18-GFP at centromeres was significantly reduced in *sad1-4A* cells, whereas Mis6-GFP enrichment was unaffected (Figures 5D and 5E). The Sad1-4A mutant protein is unable to directly recruit Mis18C to SPBs but does not detectably perturb centromere clustering at SPBs. Nonetheless, genetic analysis showed that as with Sad1-TEV140-3V5 cleavage, the *sad1-4A* mutation enhanced the TBZ sensitivity of cells when combined with *csi1* or *bub1* gene deletions, both of which have roles in chromosome segregation (Figures 5A and S5H). However, deletion of *lem2* showed no genetic interaction with *sad1-4A* (Figure S5I). Such phenotypes are consistent with compromised centromere function in *sad1-4A* cells and suggest that direct Sad1-Mis18 binding contributes to functions at centromeres that are distinct from SPB-centromere clustering.

Sad1-Mis18 association promotes CENP-A^{Cnp1} chromatin establishment and maintenance

A key function of Mis18C is to direct CENP-A^{Cnp1} deposition and thus its maintenance at centromeres.[2] We therefore tested if CENP-A^{Cnp1} incorporation at endogenous centromeres is compromised when Mis18 association with Sad1 is disrupted. However, qChIP revealed no reduction in CENP-A^{Cnp1} levels on the central domain of *cen2* (*cc2*) in *sad1-4A* cells relative to WT (Figure 6A).

In addition to CENP-A^{Cnp1} maintenance at endogenous centromeres, Mis18C may also be required to establish

(D) Localization of Mis18-GFP (top) or Mis6-GFP (bottom) and SPB protein Sid4-mCherry in *csi1Δ* DAPI stained cells (wild type in Figure S4E). Red arrows indicate centromeres (Mis6-GFP) not at SPBs in *csi1Δ* cells. Scale bar: 5 μm.
(E) Quantification of cells (%, cell number n below) with 1, 2, or 3 Mis6-GFP or Mis18-GFP foci in wild-type (WT) and *csi1Δ* cells. p value calculated by χ^2 test. See also Figure S4.

CellPress
OPEN ACCESS

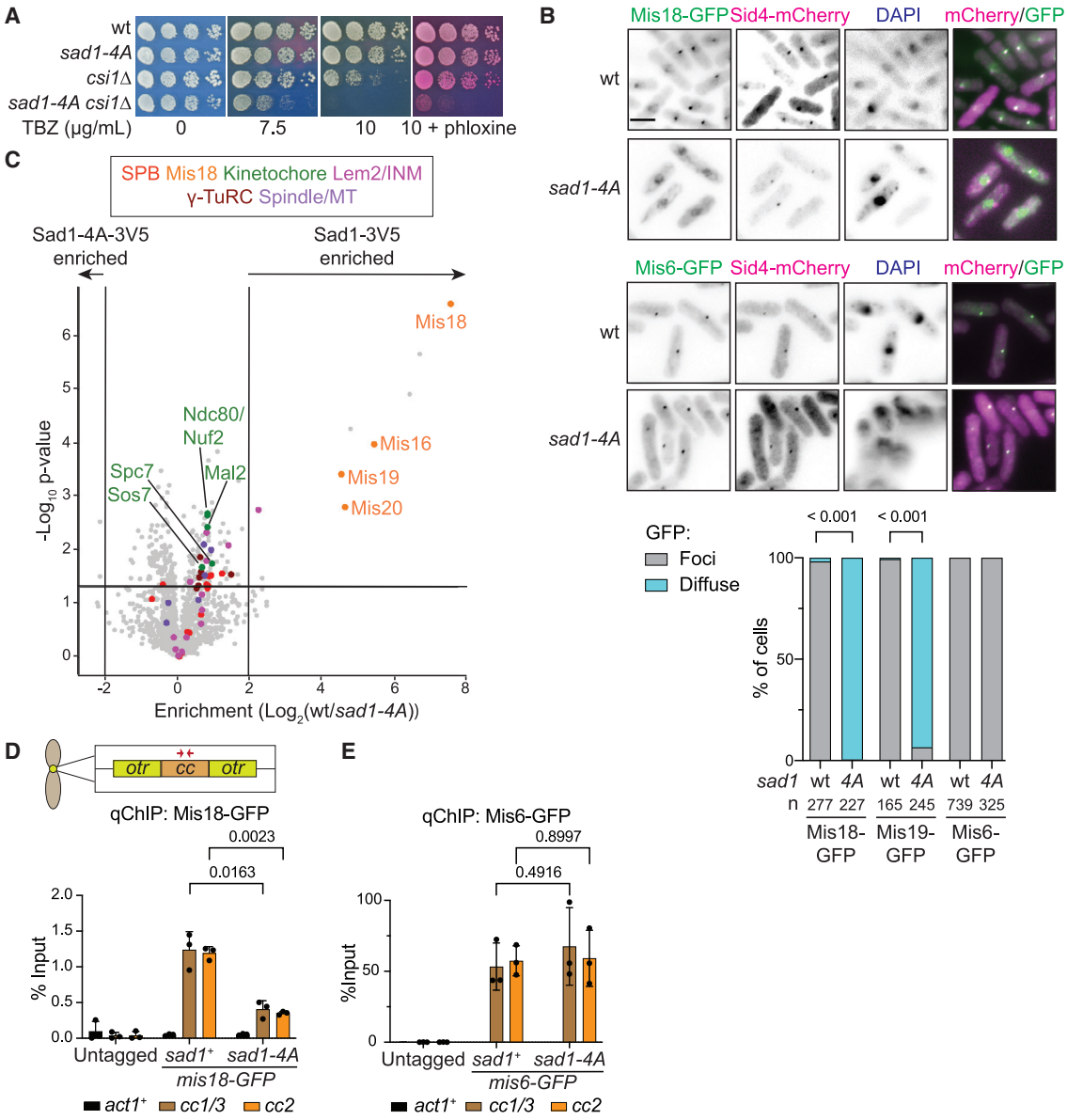

Figure 5. The *sad1-4A* mutation disperses Mis18, but not centromeres, from SPBs

(A) Serial dilution growth assays of wild-type, *sad1-4A*, *csi1Δ*, and *sad1-4A csi1Δ* cells plated on yeast extract with supplement (YES) media with or without TBZ added at the indicated concentrations. Phloxine red staining indicates inviable cells.

(B) Localization of Mis18-GFP (top), Mis6-GFP (middle), or Eic1/Mis19-GFP (see Figure S5E) and SPB protein Sid4-mCherry in wild-type (WT) or *sad1-4A* DAPI stained cells. Scale bar: 5 μm. Bottom: quantification of cells (%, cell number n below) with Mis18-GFP, Eic1/Mis19-GFP or Mis6-GFP foci or diffuse signals in wild-type (WT) and *sad1-4A* cells. p values calculated by χ^2 test.

(C) Volcano plot of LFQ-MS data comparing proteins enriched in anti-V5 Sad1-4A-3V5 and Sad1-3V5 triplicate IPs.

(D and E) Anti-GFP ChIP-qPCR for Mis18-GFP (D) and Mis6-GFP (E) on central core domains of centromeres (*cc1/3* and *cc2*, red arrows) and *act1* control locus (actin) in *sad1*$^+$ wild-type and *sad1-4A* cells and wild-type cells with no GFP (Untagged). Bar plots show mean values with standard deviation. p values calculated with Welch's t test. n = 3 biological replicates for each condition. Volcano plot protein category components are listed in Table S1 and color coded as indicated. See also Figure S5 and Data S3A and S3B.

CENP-A^{Cnp1} chromatin on naive centromere DNA templates. We therefore used a minichromosome-based establishment assay to test if SPB-associated Mis18 is required for *de novo* CENP-A^{Cnp1} chromatin assembly.[61] pHcc2 minichromosome DNA, bearing a central *cc2* core and flanking outer repeat, efficiently incorporated CENP-A^{Cnp1} on *cc2* upon transformation into WT but not *clr4*Δ negative control cells (Figure 6B). In *sad1-4A* cells, the levels of CENP-A^{Cnp1} chromatin assembled on *cc2* in pHcc2 transformants were significantly reduced relative to WT. There was considerable variability in CENP-A^{Cnp1} levels incorporated across 11 independent transformants, indicating that *de novo* CENP-A^{Cnp1} establishment was reduced but not eliminated in

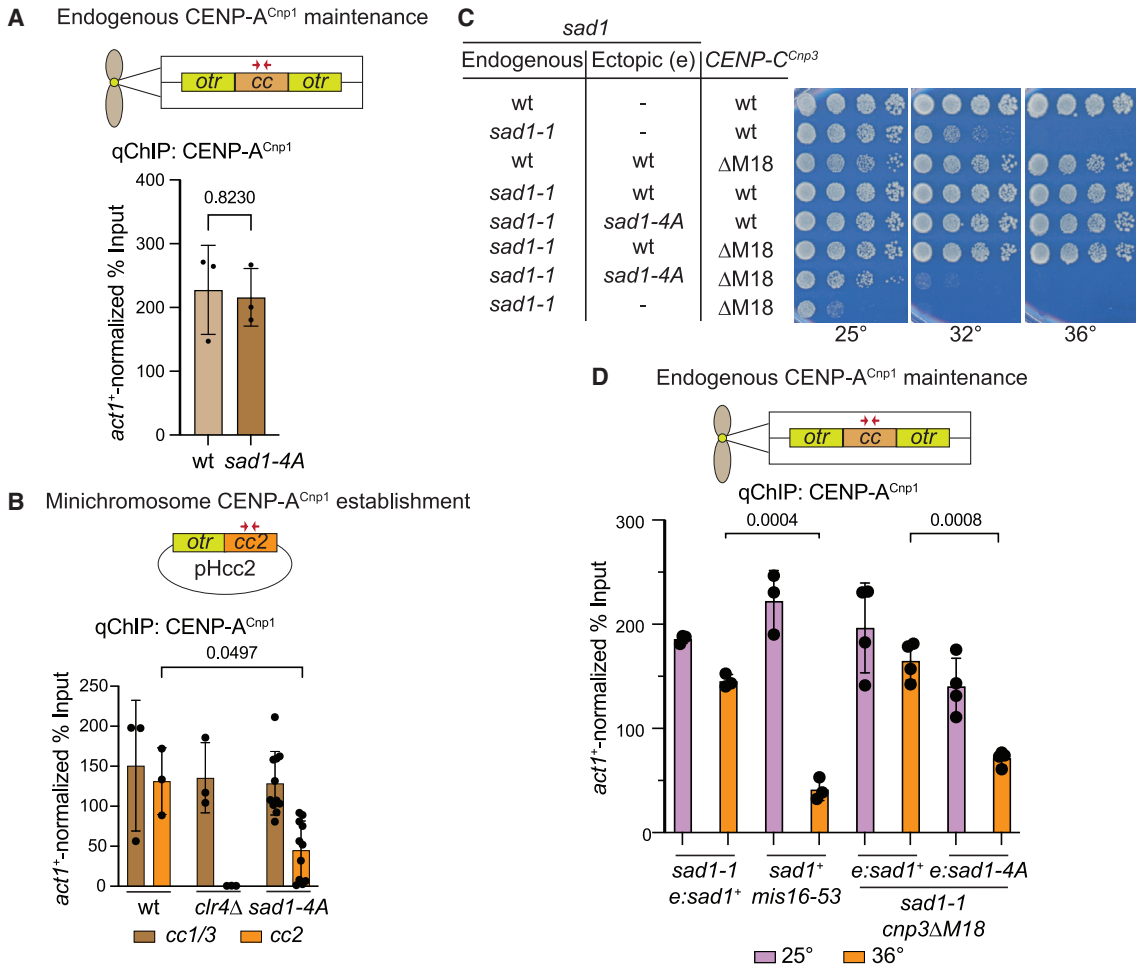

Figure 6. Mis18 utilizes Sad1 and CENP-C^{Cnp3} for CENP-A^{Cnp1} incorporation at centromeres

(A) Quantitative anti-CENP-A^{Cnp1} ChIP-qPCR for CENP-A^{Cnp1} on central core domains of centromeres (*cc1/3*, red arrows) in wild-type and *sad1-4A* cells normalized relative to *act1* locus (actin). n = 3 biological replicates for each condition.

(B) pHcc2 minichromosome DNA was transformed into wild-type, *clr4Δ* and *sad1-4A* cells. Anti-CENP-A^{Cnp1} ChIP-qPCR was performed to assess the levels of CENP-A^{Cnp1} chromatin established on the central *cc2* domain (red arrows) and control endogenous centromeric *cc1/3* loci in multiple individual pHcc2 transformants relative to CENP-A^{Cnp1} on the *act1* control locus. *cc2* is unique to pHcc2 in these cells because endogenous *cc2* is replaced with *cc1*.[61] n = 3 biological replicates for wild type and *clr4Δ*, and n = 11 for *sad1-4A*.

(C) Serial dilution growth assays of the indicated strains plated on YES media at 25°C, 32°C, or 36°C.

(D) Anti-CENP-A^{Cnp1} ChIP-qPCR performed to assess the level of CENP-A^{Cnp1} chromatin on the endogenous central *cc2* domain of *cen2* (red arrows) relative to the *act1* control locus in cells with the temperature-sensitive *sad1-1* mutation covered by ectopically integrated *sad1*$^+$ or *sad1-4A* genes. Cells grown at 25°C were shifted to 36°C prior to fixation. Error bars: SD. p values: Welch's t test. n = 4 biological replicates for *cnp3ΔM18* samples, and n = 3 for all others.

See also Figure S6.

sad1-4A cells. Thus, although the SPB-Sad1-associated Mis18 pool is not required to maintain existing CENP-A^{Cnp1} at endogenous centromeres, it ensures that CENP-A^{Cnp1} chromatin can be efficiently established when CENP-A^{Cnp1} and kinetochore proteins are initially absent from substrate DNA.

sad1-4A cells are viable, despite the loss of Mis18 from SPBs, whereas Mis18 is essential for viability.[21] Moreover, the retention of some Mis18 at centromeres in *sad1-4A* cells (Figure 5D) suggests the existence of a separate centromere-based Mis18 recruitment pathway that may permit CENP-A^{Cnp1} maintenance and *sad1-4A* viability when the main SPB-Sad1-associated Mis18 pool is dispersed. *S. pombe* Mis18 is known to bind CENP-C^{Cnp3}, and disruption of this interaction in *cnp3ΔM18* (residues 325–490 removed) mutant cells results in slow growth, TBZ sensitivity (Figures S6A and S6B), and lower CENP-A^{Cnp1} signals at centromeres.[31] Growth of *cnp3ΔM18* cells was also inhibited when Mis18C was released from SPBs by Sad1-TEV60-3V5 cleavage (Figure S6A). Moreover, genetic analysis demonstrated that *sad4-A cnp3ΔM18* double-mutant cells are not viable (Figure S6C). These genetic interactions are consistent with the operation of distinct SPB-Sad1- and centromere-CENP-C^{Cnp3}-based pathways for Mis18C recruitment to SPB-centromere clusters.

We therefore used the *cnp3ΔM18* mutation to test if disruption of CENP-C^{Cnp3}-Mis18 association renders CENP-A^{Cnp1} chromatin assembly dependent upon the main Sad1-associated Mis18 pool.

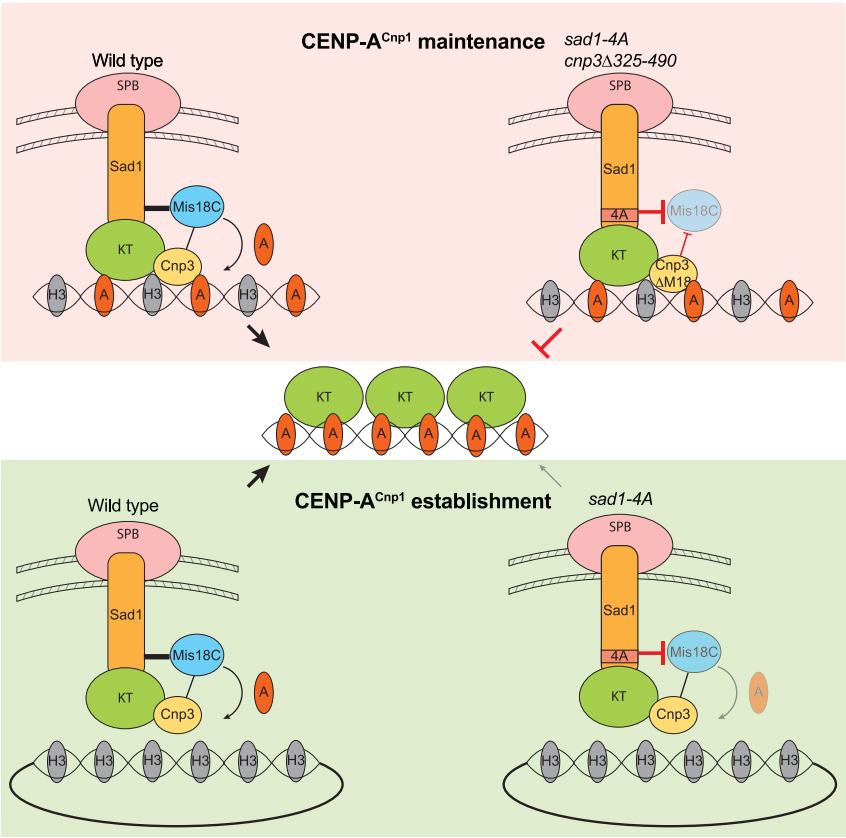

Figure 7. Model showing parallel Sad1 and CENP-C^{Cnp3} pathways of Mis18 recruitment and CENP-A^{Cnp1} incorporation

Endogenous centromeres are maintained by Mis18C recruitment to SPBs through Sad1 and centromeres via CENP-C^{Cnp3}. Most Mis18C localizes to SPB-centromere clusters through direct association with Sad1 (thick line) and a small proportion is recruited to centromeres via CENP-C^{Cnp3} (thin line). Mis18C recruitment is abolished in *sad1-4A cnp3ΔM18* cells, which inhibits CENP-A^{Cnp1} assembly at endogenous centromeres, causing lethality. *De novo* CENP-A^{Cnp1} chromatin assembly and centromere formation on minichromosomes bearing appropriate DNA occurs when they are in close proximity to SPBs and therefore Mis18C. Mis18C association with SPBs is disrupted in *sad1-4A* cells leading to defective *de novo* CENP-A^{Cnp1} chromatin assembly (light arrow).

cnp3ΔM18 cells bearing the *sad1-1* temperature-sensitive mutation were constructed with the *sad1* gene promoter driving either WT Sad1 or Sad1-4A protein expression from an ectopic locus (*e*). Shifting these cells to 36°C inactivates Sad1-1, allowing the phenotype of *e:sad4-A cnp3ΔM18* double mutants to be assessed relative to e:*sad1*$^{+}$ *cnp3ΔM18* cells. As expected, *sad1-1 e:sad1*$^{+}$ *cnp3ΔM18* cells were viable at both permissive (25°C) and restrictive (36°C) temperatures. In contrast, *sad1-1 e:sad4-A cnp3ΔM18* were inviable at 36°C, although Sad1-4A was expressed at similar levels to WT Sad1 (Figures 6C and S6D). qChIP revealed that the levels of CENP-A^{Cnp1} on endogenous centromeres was significantly reduced in *sad1-1* e:*sad1-4A cnp3ΔM18* relative to *sad1-1* e:*sad1*$^{+}$ *cnp3ΔM18* cells at 36°C (Figure 6D). Similarly, CENP-A^{Cnp1} centromere levels were depleted in *mis16-53* mutant cells that lose Mis18C function at 36°C (Figure 6D).[21] Thus, the *sad4-A* and *cnp3ΔM18* mutations act synergistically to impair CENP-A^{Cnp1} incorporation. We conclude that two pathways operate to efficiently recruit Mis18 to centromeres and ensure maintenance of normal CENP-A^{Cnp1} levels (Figure 7): one through direct association of Mis18 with Sad1 at SPBs and the other via CENP-C^{Cnp3} at centromeres.

DISCUSSION

Mis18C is required to maintain CENP-A chromatin, and thus kinetochore integrity, by targeting the CENP-A chaperone HJURP to pre-existing CENP-A chromatin. To understand how centromeres are established and propagated, and how neocentromere formation is suppressed, it is important to determine how Mis18C is recruited to its chromatin substrate. In mammalian cells, Mis18α/β are recruited to pre-existing CENP-A chromatin by binding the adaptor protein M18BP1, which associates with CENP-C at existing centromeres. However, various eukaryotes, including *S. pombe* and *D. melanogaster*, lack a M18BP1 ortholog, suggesting that other mechanisms of Mis18 recruitment are of primary importance in these systems and that similar mechanisms may also contribute to CENP-A chromatin maintenance even in species exhibiting the canonical Mis18α/β-M18BP1 pathway.[25,62–65] In many organisms, centromeres tend to cluster, a phenomenon that is particularly prevalent in various fungi and plants where centromeres cluster near SPBs.[33–35,66,67] Here, we demonstrate that in fission yeast, Mis18C is directly recruited to SPBs, thereby concentrating it near centromeres that robustly cluster near SPBs in G2 cells when CENP-A^{Cnp1} is replenished. Our analyses show that this Mis18-SPB pathway is needed for efficient CENP-A chromatin establishment on centromere DNA and also acts in parallel to a conventional Mis18-CENP-C^{Cnp3} pathway to preserve CENP-A^{Cnp1} chromatin at centromeres.

Our TEV-induced cleavage strategy identified proteins that specifically associate with the N-terminal nucleoplasmic region of Sad1, providing insight into the constituents on the nucleoplasmic side of *S. pombe* SPBs (Figures 1 and 2). Components of Mis18C were found to associate with Sad1 via its N-terminal 60 residues. Mis18C association with Sad1 involves direct binding of Mis18 with Sad1, and this interaction was disrupted by the specific *sad1-4A* N-terminal mutation. In contrast, the Lem2 and Csi1 proteins, which are known to contribute to SPB-centromere clustering, appeared to associate with Sad1 through residues 60–140 and 140–167, respectively. This modular arrangement suggests that Mis18C recruitment and SPB-centromere clustering are separable Sad1 functions. Indeed, the *sad1-4A* mutation dispersed most Mis18-GFP away from SPBs without affecting centromere (Mis6-GFP) clustering at SPBs (Figure 5B). Reciprocally, most Mis18-GFP remained at SPBs and did not

colocalize with centromeres, which had separated from G2 SPBs in *csi1*Δ cells (Figure 4E). Thus, the congregation of centromeres at SPBs and Mis18C recruitment to SPB-centromere clusters are mediated by distinct segments of the Sad1 nucleoplasmic region.

Sad1 is located at SPBs throughout the cell cycle, whereas Mis18C is released from the SPB-centromere cluster upon mitotic entry,[21,24,47] suggesting that association of Mis18 with Sad1 might be regulated by post-translational modification. *S. pombe* Cdk1 (Cdc2) and Polo (Plo1) kinases are active at SPBs upon mitotic onset, just after maximal CENP-A^{Cnp1} incorporation in late G2, when Mis18 is released from SPBs.[17,18,68] Mitotic phosphorylation of both Sad1 and Mis18 have been reported,[69,70] and Plo1 kinase activity is required to reconfigure Sad1 into a ring around SPBs at the end of G2.[71] Since unphosphorylated recombinant Mis18 directly associates with the Sad1 N-terminal region *in vitro* (Figures 4A and 4B), we surmise that phosphorylation of Sad1 and/or Mis18 may disrupt their association to coordinate release of Mis18C from SPBs with disengagement of centromeres, mitotic entry, and spindle formation. Interestingly, the association of hMis18α with the hM18BP1 adapter protein in human cells has been shown to be regulated by Polo and Cdk1 kinase-mediated phosphorylation—promoting and preventing their association, respectively.[26,72–75]

Association of the conserved Yippee domain of hMis18α with hM18BP1 is required for hMis18α recruitment to human centromeres.[25,26,30,74] As our structural analyses predict that the Yippee domain of *S. pombe* Mis18 mediates its interaction with the Sad1 N-terminal region (Figure 4C), we conclude that Sad1 performs the equivalent function of human M18BP1 in mediating *S. pombe* Mis18C recruitment.[26,27,30,74] Our findings that neither the N- nor C-terminal domains of Mis18 were sufficient to bind the Sad1 nucleoplasmic region *in vitro* (Figure S4A) and that the short Mis18 ct was required for robust binding (Figures S4B–S4D) suggest that additional binding interactions between Mis18 and Sad1 may exist. It is also possible that the N-terminal portion of Mis18 (Mis18-N) alone does not adopt a native conformation, explaining its inability to bind MBP-Sad1-N *in vitro* (Figure S4A).

Because Mis18 is required for the assembly of CENP-A^{Cnp1} chromatin,[21] our discovery of a direct Mis18-Sad1 interaction suggested that *S. pombe* SPBs might provide a platform to ensure CENP-A^{Cnp1} replenishment during G2. Disruption of either the Mis18-Sad1 interaction (*sad1-4A*; Figure 6A) or Mis18 recruitment to centromeres via CENP-C^{Cnp3} (*cnp3ΔM18*; Figure 6D)[31] did not impact CENP-A^{Cnp1} levels at endogenous centromeres. However, combining *sad1-4A* and *cnp3ΔM18* in conditionally mutant cells resulted in lower CENP-A^{Cnp1} levels at centromeres and lethality (Figures 6C and 6D). Although CENP-A^{Cnp1} was still detectable at centromeres in this conditional strain, this was also the case for control *mis16-53* cells (Figure 6D). Low levels of CENP-A^{Cnp1} are expected to remain at centromeres after the 8-h temperature shift because pre-existing CENP-A^{Cnp1} will be retained but diluted through each S phase in the absence of new CENP-A^{Cnp1} deposition. We therefore interpret the observed decrease in CENP-A^{Cnp1} levels at centromere as indicating a strong defect in Mis18C function in both *mis16-53* and *sad1-4A cnp3ΔM18* conditional mutants. These observations indicate that the SPB-Sad1-Mis18 pathway identified here operates redundantly with a centromere-based CENP-C^{Cnp3}-Mis18 pathway to maintain CENP-A^{Cnp1} chromatin. We also observed significantly lower levels of CENP-A^{Cnp1} chromatin establishment on naive minichromosome-borne centromere DNA (Figure 6B) in *sad1-4A* cells, demonstrating that Mis18-Sad1 association is required to promote robust *de novo* CENP-A^{Cnp1} chromatin assembly (Figure 7).

S. pombe pericentromeric heterochromatin appears to localize the central core domain of centromeres to the nuclear periphery, where it can encounter existing centromeres at SPBs and promote efficient *de novo* CENP-A^{Cnp1} chromatin assembly.[41,42,61] Moreover, inserting a naive centromeric DNA template near an existing centromere or tethering a plasmid with naive centromeric DNA to SPBs promotes CENP-A^{Cnp1} establishment independently of flanking heterochomatin.[41] These findings led us to propose that the centromere cluster provides a microenvironment where CENP-A^{Cnp1} assembly factors (Mis18C and HJURP^{Scm3}) are concentrated, promoting CENP-A^{Cnp1} chromatin establishment and maintenance. However, unexpectedly, we find that the N-terminal region of Sad1 recruits Mis18C independently of centromeres or their clustering, thereby providing two-factor authentication in centromere specification: naive centromeric DNA exhibiting appropriate properties and positioned in the right nuclear location (near SPBs) establishes CENP-A^{Cnp1} chromatin more efficiently.

Interestingly, centromeres cluster at the nuclear periphery in normal human tissues, and this clustering decreases in cancer cells,[10] which frequently also exhibit aberrant CENP-A expression and centromere locations. The Mis18-Sad1-SPB recruitment mechanism we have uncovered here reveals how centromere identity is ensured through the spatial positioning of centromeres in nuclei. It is possible that centromere clustering in human and other cell types also contributes to their establishment and maintenance.

STAR★METHODS

Detailed methods are provided in the online version of this paper and include the following:

- KEY RESOURCES TABLE
- RESOURCE AVAILABILITY
  - Lead contact
  - Materials availability
  - Data and code availability
- EXPERIMENTAL MODEL AND SUBJECT DETAILS
  - Yeast strain construction
  - Yeast growth conditions
- METHOD DETAILS
  - Cloning
  - Protein expression
  - Protein purification and size exclusion chromatography
  - Protein binding assays
  - qChIP
  - Immunoprecipitation
  - Mass spectrometry
  - qChIP
  - Immunofluorescence

- Microscopy and image analysis
- QUANTIFICATION AND STATISTICAL ANALYSIS

SUPPLEMENTAL INFORMATION

Supplemental information can be found online at https://doi.org/10.1016/j.cub.2023.08.063.

ACKNOWLEDGMENTS

We thank members of team Allshire for input during the course of this work, especially Alison L. Pidoux for suggesting the TEV cleavage strategy and insightful comments on the manuscript. We thank Dave Kelly and Toni McHugh for training on, and maintenance of, our microscopes, Ken Sawin for anti-Cdc11 antibody, the Marston lab for plasmid carrying the TEV protease sequence, Mitsuhiro Yanagida for *mis16-GFP* and *mis18-GFP* strains, Sigurd Braun for the *lem2*Δ strain, and Iain Hagan for providing Keith Gull's Tat1 antibody. The Edinburgh Protein Production Facility provided protein purification equipment (Wellcome Multi-User Equipment grant 101527).

This work was funded by an HHMI Life Sciences Research Foundation Award to N.L., consecutive Wellcome Principal Research Fellowships to R.C.A. supporting N.L. (224358 and 200885), a Wellcome Senior Research Fellowship (202811), an ERC advanced grant (CHROMSEG, 101054950) to A.A.J. supporting B.M.-P., a Wellcome Instrument grant to J.R. (108504), and core funding for the Wellcome Centre for Cell Biology (203149) supporting C.S.

AUTHOR CONTRIBUTIONS

N.L. and R.C.A. conceived the study. Experiments were performed by N.L. B.M.-P. provided recombinant proteins. B.M.-P. and J.P. contributed to experimental design. C.S. performed mass spectrometry and initial data processing facilitated by J.R. N.L. and R.C.A wrote the manuscript.

DECLARATION OF INTERESTS

The authors declare no competing interests.

Received: June 21, 2023
Revised: August 4, 2023
Accepted: August 22, 2023
Published: September 14, 2023

REFERENCES

1. Allshire, R.C., and Karpen, G.H. (2008). Epigenetic regulation of centromeric chromatin: old dogs, new tricks? Nat. Rev. Genet. *9*, 923–937. https://doi.org/10.1038/nrg2466.
2. McKinley, K.L., and Cheeseman, I.M. (2016). The molecular basis for centromere identity and function. Nat. Rev. Mol. Cell Biol. *17*, 16–29. https://doi.org/10.1038/nrm.2015.5.
3. Ishii, K., Ogiyama, Y., Chikashige, Y., Soejima, S., Masuda, F., Kakuma, T., Hiraoka, Y., and Takahashi, K. (2008). Heterochromatin integrity affects chromosome reorganization after centromere dysfunction. Science *321*, 1088–1091. https://doi.org/10.1126/science.1158699.
4. DeBose-Scarlett, E.M., and Sullivan, B.A. (2021). Genomic and epigenetic foundations of neocentromere formation. Annu. Rev. Genet. *55*, 331–348. https://doi.org/10.1146/annurev-genet-071719-020924.
5. Murillo-Pineda, M., Valente, L.P., Dumont, M., Mata, J.F., Fachinetti, D., and Jansen, L.E.T. (2021). Induction of spontaneous human neocentromere formation and long-term maturation. J. Cell Biol. *220*, https://doi.org/10.1083/jcb.202007210.
6. Ketel, C., Wang, H.S.W., McClellan, M., Bouchonville, K., Selmecki, A., Lahav, T., Gerami-Nejad, M., and Berman, J. (2009). Neocentromeres form efficiently at multiple possible loci in Candida albicans. PLoS Genet. *5*, e1000400. https://doi.org/10.1371/journal.pgen.1000400.
7. Shang, W.H., Hori, T., Martins, N.M.C., Toyoda, A., Misu, S., Monma, N., Hiratani, I., Maeshima, K., Ikeo, K., Fujiyama, A., et al. (2013). Chromosome engineering allows the efficient isolation of vertebrate neocentromeres. Dev. Cell *24*, 635–648. https://doi.org/10.1016/j.devcel.2013.02.009.
8. Lu, M., and He, X. (2019). Centromere repositioning causes inversion of meiosis and generates a reproductive barrier. Proc. Natl. Acad. Sci. USA *116*, 21580–21591. https://doi.org/10.1073/pnas.1911745116.
9. Murillo-Pineda, M., and Jansen, L.E.T. (2020). Genetics, epigenetics and back again: lessons learned from neocentromeres. Exp. Cell Res. *389*, 111909. https://doi.org/10.1016/j.yexcr.2020.111909.
10. Verrelle, P., Meseure, D., Berger, F., Forest, A., Leclère, R., Nicolas, A., Fortas, E., Sastre-Garau, X., Lae, M., Boudjemaa, S., et al. (2021). CENP-A subnuclear localization pattern as marker predicting curability by chemo-radiation therapy for locally advanced head and neck cancer patients. Cancers (Basel) *13*, 3928. https://doi.org/10.3390/cancers13163928.
11. Zhang, W., Mao, J.H., Zhu, W., Jain, A.K., Liu, K., Brown, J.B., and Karpen, G.H. (2016). Centromere and kinetochore gene misexpression predicts cancer patient survival and response to radiotherapy and chemotherapy. Nat. Commun. *7*, 12619. https://doi.org/10.1038/ncomms12619.
12. Choi, E.S., Strålfors, A., Catania, S., Castillo, A.G., Svensson, J.P., Pidoux, A.L., Ekwall, K., and Allshire, R.C. (2012). Factors that promote H3 chromatin integrity during transcription prevent promiscuous deposition of CENP-A(Cnp1) in fission yeast. PLoS Genet. *8*, e1002985. https://doi.org/10.1371/journal.pgen.1002985.
13. Collins, K.A., Furuyama, S., and Biggins, S. (2004). Proteolysis contributes to the exclusive centromere localization of the yeast Cse4/CENP-A histone H3 variant. Curr. Biol. *14*, 1968–1972. https://doi.org/10.1016/j.cub.2004.10.024.
14. Dong, Q., Yang, J., Gao, J., and Li, F. (2021). Recent insights into mechanisms preventing ectopic centromere formation. Open Biol. *11*, 210189. https://doi.org/10.1098/rsob.210189.
15. Jansen, L.E.T., Black, B.E., Foltz, D.R., and Cleveland, D.W. (2007). Propagation of centromeric chromatin requires exit from mitosis. J. Cell Biol. *176*, 795–805. https://doi.org/10.1083/jcb.200701066.
16. Dunleavy, E.M., Pidoux, A.L., Monet, M., Bonilla, C., Richardson, W., Hamilton, G.L., Ekwall, K., McLaughlin, P.J., and Allshire, R.C. (2007). A NASP (N1/N2)-related protein, Sim3, binds CENP-A and is required for its deposition at fission yeast centromeres. Mol. Cell *28*, 1029–1044. https://doi.org/10.1016/j.molcel.2007.10.010.
17. Lando, D., Endesfelder, U., Berger, H., Subramanian, L., Dunne, P.D., McColl, J., Klenerman, D., Carr, A.M., Sauer, M., Allshire, R.C., et al. (2012). Quantitative single-molecule microscopy reveals that CENP-A(Cnp1) deposition occurs during G2 in fission yeast. Open Biol. *2*, 120078. https://doi.org/10.1098/rsob.120078.
18. Shukla, M., Tong, P., White, S.A., Singh, P.P., Reid, A.M., Catania, S., Pidoux, A.L., and Allshire, R.C. (2018). Centromere DNA destabilizes H3 nucleosomes to promote CENP-A deposition during the cell cycle. Curr. Biol. *28*, 3924–3936.e4. https://doi.org/10.1016/j.cub.2018.10.049.
19. Takayama, Y., Sato, H., Saitoh, S., Ogiyama, Y., Masuda, F., and Takahashi, K. (2008). Biphasic incorporation of centromeric histone CENP-A in fission yeast. Mol. Biol. Cell *19*, 682–690. https://doi.org/10.1091/mbc.e07-05-0504.
20. Takahashi, K., Takayama, Y., Masuda, F., Kobayashi, Y., and Saitoh, S. (2005). Two distinct pathways responsible for the loading of CENP-A to centromeres in the fission yeast cell cycle; discussion 606. Philos. Trans. R. Soc. Lond. B Biol. Sci. *360*, 595–606. https://doi.org/10.1098/rstb.2004.1614.
21. Hayashi, T., Fujita, Y., Iwasaki, O., Adachi, Y., Takahashi, K., and Yanagida, M. (2004). Mis16 and Mis18 are required for CENP-A loading and histone deacetylation at centromeres. Cell *118*, 715–729. https://doi.org/10.1016/j.cell.2004.09.002.
22. Hayashi, T., Ebe, M., Nagao, K., Kokubu, A., Sajiki, K., and Yanagida, M. (2014). Schizosaccharomyces pombe centromere protein Mis19 links Mis16 and Mis18 to recruit CENP-A through interacting with NMD factors

and the SWI/SNF complex. Genes Cells *19*, 541–554. https://doi.org/10.1111/gtc.12152.

23. Hirai, H., Arai, K., Kariyazono, R., Yamamoto, M., and Sato, M. (2014). The kinetochore protein Kis1/Eic1/Mis19 ensures the integrity of mitotic spindles through maintenance of kinetochore factors Mis6/CENP-I and CENP-A. PLoS One *9*, e111905. https://doi.org/10.1371/journal.pone.0111905.
24. Subramanian, L., Toda, N.R.T., Rappsilber, J., and Allshire, R.C. (2014). Eic1 links Mis18 with the CCAN/Mis6/Ctf19 complex to promote CENP-A assembly. Open Biol. *4*, 140043. https://doi.org/10.1098/rsob.140043.
25. Fujita, Y., Hayashi, T., Kiyomitsu, T., Toyoda, Y., Kokubu, A., Obuse, C., and Yanagida, M. (2007). Priming of centromere for CENP-A recruitment by human hMis18α, hMis18β, and M18BP1. Dev. Cell *12*, 17–30. https://doi.org/10.1016/j.devcel.2006.11.002.
26. Pan, D., Klare, K., Petrovic, A., Take, A., Walstein, K., Singh, P., Rondelet, A., Bird, A.W., and Musacchio, A. (2017). CDK-regulated dimerization of M18BP1 on a Mis18 hexamer is necessary for CENP-A loading. eLife *6*, e23352. https://doi.org/10.7554/eLife.23352.
27. Stellfox, M.E., Nardi, I.K., Knippler, C.M., and Foltz, D.R. (2016). Differential binding partners of the Mis18α/β YIPPEE domains regulate Mis18 complex recruitment to centromeres. Cell Rep. *15*, 2127–2135. https://doi.org/10.1016/j.celrep.2016.05.004.
28. Jiang, H., Ariyoshi, M., Hori, T., Watanabe, R., Makino, F., Namba, K., and Fukagawa, T. (2023). The cryo-EM structure of the CENP-A nucleosome in complex with ggKNL2. EMBO J. *42*, e111965. https://doi.org/10.15252/embj.2022111965.
29. Mellone, B.G., and Fachinetti, D. (2021). Diverse mechanisms of centromere specification. Curr. Biol. *31*, R1491–R1504. https://doi.org/10.1016/j.cub.2021.09.083.
30. Thamkachy, R., Medina-Pritchard, B., Park, S.H., Zou, J., Páramo, C.G., Feederle, R., Ruksenaite, E., Davies, O.R., Rappsilber, J., Schneidman-Duhovny, D., et al. Structural basis for Mis18 complex assembly: implications for centromere maintenance. Preprint at bioRxiv. https://doi.org/10.1101/2021.11.08.466737.
31. Zhang, M., Zheng, F., Xiong, Y., Shao, C., Wang, C., Wu, M., Niu, X., Dong, F., Zhang, X., Fu, C., et al. (2021). Centromere targeting of Mis18 requires the interaction with DNA and H2A–H2B in fission yeast. Cell. Mol. Life Sci. *78*, 373–384. https://doi.org/10.1007/s00018-020-03502-1.
32. Tanaka, K., Chang, H.L., Kagami, A., and Watanabe, Y. (2009). CENP-C functions as a scaffold for effectors with essential kinetochore functions in mitosis and meiosis. Dev. Cell *17*, 334–343. https://doi.org/10.1016/j.devcel.2009.08.004.
33. Funabiki, H., Hagan, I., Uzawa, S., and Yanagida, M. (1993). Cell cycle-dependent specific positioning and clustering of centromeres and telomeres in fission yeast. J. Cell Biol. *121*, 961–976. https://doi.org/10.1083/jcb.121.5.961.
34. Hoencamp, C., Dudchenko, O., Elbatsh, A.M.O., Brahmachari, S., Raaijmakers, J.A., van Schaik, T., Sedeño Cacciatore, Á., Contessoto, V.G., van Heesbeen, R.G.H.P., van den Broek, B., et al. (2021). 3D genomics across the tree of life reveals condensin II as a determinant of architecture type. Science *372*, 984–989. https://doi.org/10.1126/science.abe2218.
35. Oko, Y., Ito, N., and Sakamoto, T. (2020). The mechanisms and significance of the positional control of centromeres and telomeres in plants. J. Plant Res. *133*, 471–478. https://doi.org/10.1007/s10265-020-01202-2.
36. Cavanaugh, A.M., and Jaspersen, S.L. (2017). Big lessons from little yeast: budding and fission yeast centrosome structure, duplication, and function. Annu. Rev. Genet. *51*, 361–383. https://doi.org/10.1146/annurev-genet-120116-024733.
37. Franco, A., Meadows, J.C., and Millar, J.B.A. (2007). The Dam1/DASH complex is required for the retrieval of unclustered kinetochores in fission yeast. J. Cell Sci. *120*, 3345–3351. https://doi.org/10.1242/jcs.013698.
38. Hou, H., Zhou, Z., Wang, Y., Wang, J., Kallgren, S.P., Kurchuk, T., Miller, E.A., Chang, F., and Jia, S. (2012). Csi1 links centromeres to the nuclear envelope for centromere clustering. J. Cell Biol. *199*, 735–744. https://doi.org/10.1083/jcb.201208001.
39. Hou, H., Kallgren, S.P., and Jia, S. (2013). Csi1 illuminates the mechanism and function of Rabl configuration. Nucleus *4*, 176–181. https://doi.org/10.4161/nucl.24876.
40. Tanaka, K., Mukae, N., Dewar, H., van Breugel, M., James, E.K., Prescott, A.R., Antony, C., and Tanaka, T.U. (2005). Molecular mechanisms of kinetochore capture by spindle microtubules. Nature *434*, 987–994. https://doi.org/10.1038/nature03483.
41. Wu, W., McHugh, T., Kelly, D.A., Pidoux, A.L., and Allshire, R.C. (2022). Establishment of centromere identity is dependent on nuclear spatial organization. Curr. Biol. *32*, 3121–3136.e6. https://doi.org/10.1016/j.cub.2022.06.048.
42. Pidoux, A.L., Choi, E.S., Abbott, J.K.R., Liu, X., Kagansky, A., Castillo, A.G., Hamilton, G.L., Richardson, W., Rappsilber, J., He, X., et al. (2009). Fission yeast Scm3: a CENP-A receptor required for integrity of subkinetochore chromatin. Mol. Cell *33*, 299–311. https://doi.org/10.1016/j.molcel.2009.01.019.
43. Williams, J.S., Hayashi, T., Yanagida, M., and Russell, P. (2009). Fission yeast Scm3 mediates stable assembly of Cnp1/CENP-A into centromeric chromatin. Mol. Cell *33*, 287–298. https://doi.org/10.1016/j.molcel.2009.01.017.
44. Bestul, A.J., Yu, Z., Unruh, J.R., and Jaspersen, S.L. (2017). Molecular model of fission yeast centrosome assembly determined by superresolution imaging. J. Cell Biol. *216*, 2409–2424. https://doi.org/10.1083/jcb.201701041.
45. Ding, R., West, R.R., Morphew, D.M., Oakley, B.R., and McIntosh, J.R. (1997). The spindle pole body of Schizosaccharomyces pombe enters and leaves the nuclear envelope as the cell cycle proceeds. Mol. Biol. Cell *8*, 1461–1479. https://doi.org/10.1091/mbc.8.8.1461.
46. Gonzalez, Y., Saito, A., and Sazer, S. (2012). Fission yeast Lem2 and Man1 perform fundamental functions of the animal cell nuclear lamina. Nucleus *3*, 60–76. https://doi.org/10.4161/nucl.18824.
47. Hagan, I., and Yanagida, M. (1995). The product of the spindle formation gene sad1+ associates with the fission yeast spindle pole body and is essential for viability. J. Cell Biol. *129*, 1033–1047. https://doi.org/10.1083/jcb.129.4.1033.
48. Barrales, R.R., Forn, M., Georgescu, P.R., Sarkadi, Z., and Braun, S. (2016). Control of heterochromatin localization and silencing by the nuclear membrane protein Lem2. Genes Dev. *30*, 133–148. https://doi.org/10.1101/gad.271288.115.
49. Fernández-Álvarez, A., and Cooper, J.P. (2017). The functionally elusive Rabl chromosome configuration directly regulates nuclear membrane remodeling at mitotic onset. Cell Cycle *16*, 1392–1396. https://doi.org/10.1080/15384101.2017.1338986.
50. Goto, B., Okazaki, K., and Niwa, O. (2001). Cytoplasmic microtubular system implicated in de novo formation of a Rabl-like orientation of chromosomes in fission yeast. J. Cell Sci. *114*, 2427–2435. https://doi.org/10.1242/jcs.114.13.2427.
51. Fernández-Álvarez, A., Bez, C., O'Toole, E.T., Morphew, M., and Cooper, J.P. (2016). Mitotic nuclear envelope breakdown and spindle nucleation are controlled by interphase contacts between centromeres and the nuclear envelope. Dev. Cell *39*, 544–559. https://doi.org/10.1016/j.devcel.2016.10.021.
52. Asakawa, H., Hayashi, A., Haraguchi, T., and Hiraoka, Y. (2005). Dissociation of the Nuf2-Ndc80 complex releases centromeres from the spindle-pole body during meiotic prophase in fission yeast. Mol. Biol. Cell *16*, 2325–2338. https://doi.org/10.1091/mbc.e04-11-0996.
53. Saitoh, S., Takahashi, K., and Yanagida, M. (1997). Mis6, a fission yeast inner centromere protein, acts during G1/S and forms specialized chromatin required for equal segregation. Cell *90*, 131–143. https://doi.org/10.1016/S0092-8674(00)80320-7.
54. Zheng, F., Li, T., Jin, D., Syrovatkina, V., Scheffler, K., Tran, P.T., Fu, C., and Bloom, K.S. (2014). Csi1p recruits alp7p/TACC to the spindle pole

bodies for bipolar spindle formation. Mol. Biol. Cell *C 25*, 2750–2760. https://doi.org/10.1091/mbc.e14-03-0786.

55. Gu, M., LaJoie, D., Chen, O.S., von Appen, A., Ladinsky, M.S., Redd, M.J., Nikolova, L., Bjorkman, P.J., Sundquist, W.I., Ullman, K.S., et al. (2017). LEM2 recruits CHMP7 for ESCRT-mediated nuclear envelope closure in fission yeast and human cells. Proc. Natl. Acad. Sci. USA *114*, E2166–E2175. https://doi.org/10.1073/pnas.1613916114.
56. Kume, K., Cantwell, H., Burrell, A., and Nurse, P. (2019). Nuclear membrane protein Lem2 regulates nuclear size through membrane flow. Nat. Commun. *10*, 1871. https://doi.org/10.1038/s41467-019-09623-x.
57. Pieper, G.H., Sprenger, S., Teis, D., and Oliferenko, S. (2020). ESCRT-III/Vps4 controls heterochromatin-nuclear envelope attachments. Dev. Cell *53*, 27–41.e6. https://doi.org/10.1016/j.devcel.2020.01.028.
58. Mirdita, M., Schütze, K., Moriwaki, Y., Heo, L., Ovchinnikov, S., and Steinegger, M. (2022). ColabFold: making protein folding accessible to all. Nat. Methods *19*, 679–682. https://doi.org/10.1038/s41592-022-01488-1.
59. Subramanian, L., Medina-Pritchard, B., Barton, R., Spiller, F., Kulasegaran-Shylini, R., Radaviciute, G., Allshire, R.C., and Arockia Jeyaprakash, A. (2016). Centromere localization and function of Mis18 requires Yippee-like domain-mediated oligomerization. EMBO Rep. *17*, 496–507. https://doi.org/10.15252/embr.201541520.
60. Hiraoka, Y., Maekawa, H., Asakawa, H., Chikashige, Y., Kojidani, T., Osakada, H., Matsuda, A., and Haraguchi, T. (2011). Inner nuclear membrane protein Ima1 is dispensable for intranuclear positioning of centromeres. Genes Cells *16*, 1000–1011. https://doi.org/10.1111/j.1365-2443.2011.01544.x.
61. Folco, H.D., Pidoux, A.L., Urano, T., and Allshire, R.C. (2008). Heterochromatin and RNAi are required to establish CENP-A chromatin at centromeres. Science *319*, 94–97. https://doi.org/10.1126/science.1150944.
62. French, B.T., Westhorpe, F.G., Limouse, C., and Straight, A.F. (2017). Xenopus laevis M18BP1 directly binds existing CENP-A nucleosomes to promote centromeric chromatin assembly. Dev. Cell *42*, 190–199.e10. https://doi.org/10.1016/j.devcel.2017.06.021.
63. Hori, T., Shang, W.H., Hara, M., Ariyoshi, M., Arimura, Y., Fujita, R., Kurumizaka, H., and Fukagawa, T. (2017). Association of M18BP1/KNL2 with CENP-A nucleosome is essential for centromere formation in non-mammalian vertebrates. Dev. Cell *42*, 181–189.e3. https://doi.org/10.1016/j.devcel.2017.06.019.
64. Maddox, P.S., Hyndman, F., Monen, J., Oegema, K., and Desai, A. (2007). Functional genomics identifies a Myb domain–containing protein family required for assembly of CENP-A chromatin. J. Cell Biol. *176*, 757–763. https://doi.org/10.1083/jcb.200701065.
65. Moree, B., Meyer, C.B., Fuller, C.J., and Straight, A.F. (2011). CENP-C recruits M18BP1 to centromeres to promote CENP-A chromatin assembly. J. Cell Biol. *194*, 855–871. https://doi.org/10.1083/jcb.201106079.
66. Jin, Q.W., Fuchs, J., and Loidl, J. (2000). Centromere clustering is a major determinant of yeast interphase nuclear organization. J. Cell Sci. *113*, 1903–1912. https://doi.org/10.1242/jcs.113.11.1903.
67. Yadav, V., and Sanyal, K. (2018). Sad1 spatiotemporally regulates kinetochore clustering to ensure high-fidelity chromosome segregation in the human fungal pathogen Cryptococcus neoformans. mSphere *3*, e00190-18. https://doi.org/10.1128/mSphere.00190-18.
68. Hagan, I.M., and Grallert, A. (2013). Spatial control of mitotic commitment in fission yeast. Biochem. Soc. Trans. *41*, 1766–1771. https://doi.org/10.1042/BST20130190.
69. Koch, A., Krug, K., Pengelley, S., Macek, B., and Hauf, S. (2011). Mitotic substrates of the kinase Aurora with roles in chromatin regulation identified through quantitative phosphoproteomics of fission yeast. Sci. Signal. *4*, rs6. https://doi.org/10.1126/scisignal.2001588.
70. Swaffer, M.P., Jones, A.W., Flynn, H.R., Snijders, A.P., and Nurse, P. (2018). Quantitative phosphoproteomics reveals the signaling dynamics of cell-cycle kinases in the fission yeast Schizosaccharomyces pombe. Cell Rep. *24*, 503–514. https://doi.org/10.1016/j.celrep.2018.06.036.
71. Bestul, A.J., Yu, Z., Unruh, J.R., and Jaspersen, S.L. (2021). Redistribution of centrosomal proteins by centromeres and Polo kinase controls partial nuclear envelope breakdown in fission yeast. Mol. Biol. Cell. *32*, 1487–1500. https://doi.org/10.1091/mbc.e21-05-0239.
72. McKinley, K.L., and Cheeseman, I.M. (2014). Polo-like kinase 1 licenses CENP-A deposition at centromeres. Cell *158*, 397–411. https://doi.org/10.1016/j.cell.2014.06.016.
73. Silva, M.C.C., Bodor, D.L., Stellfox, M.E., Martins, N.M.C., Hochegger, H., Foltz, D.R., and Jansen, L.E.T. (2012). Cdk activity couples epigenetic centromere inheritance to cell cycle progression. Dev. Cell *22*, 52–63. https://doi.org/10.1016/j.devcel.2011.10.014.
74. Spiller, F., Medina-Pritchard, B., Abad, M.A., Wear, M.A., Molina, O., Earnshaw, W.C., and Jeyaprakash, A.A. (2017). Molecular basis for Cdk1-regulated timing of Mis18 complex assembly and CENP-A deposition. EMBO Rep. *18*, 894–905. https://doi.org/10.15252/embr.201643564.
75. Stankovic, A., Guo, L.Y., Mata, J.F., Bodor, D.L., Cao, X.J., Bailey, A.O., Shabanowitz, J., Hunt, D.F., Garcia, B.A., Black, B.E., et al. (2017). A dual inhibitory mechanism sufficient to maintain cell-cycle-restricted CENP-A assembly. Mol. Cell *65*, 231–246. https://doi.org/10.1016/j.molcel.2016.11.021.
76. Cox, J., and Mann, M. (2008). MaxQuant enables high peptide identification rates, individualized p.p.b.-range mass accuracies and proteome-wide protein quantification. Nat. Biotechnol. *26*, 1367–1372. https://doi.org/10.1038/nbt.1511.
77. Tyanova, S., Temu, T., and Cox, J. (2016). The MaxQuant computational platform for mass spectrometry-based shotgun proteomics. Nat. Protoc. *11*, 2301–2319. https://doi.org/10.1038/nprot.2016.136.
78. Bähler, J., Wu, J.Q., Longtine, M.S., Shah, N.G., McKenzie, A., Steever, A.B., Wach, A., Philippsen, P., and Pringle, J.R. (1998). Heterologous modules for efficient and versatile PCR-based gene targeting in Schizosaccharomyces pombe. Yeast *14*, 943–951. https://doi.org/10.1002/(SICI)1097-0061(199807)14:10<943::AID-YEA292>3.0.CO;2-Y.
79. Torres-Garcia, S., Di Pompeo, L., Eivers, L., Gaborieau, B., White, S.A., Pidoux, A.L., Kanigowska, P., Yaseen, I., Cai, Y., and Allshire, R.C. (2020). SpEDIT: a fast and efficient CRISPR/Cas9 method for fission yeast. Wellcome Open Res. *5*, 274. https://doi.org/10.12688/wellcomeopenres.16405.1.
80. Maundrell, K. (1993). Thiamine-repressible expression vectors pREP and pRIP for fission yeast. Gene *123*, 127–130. https://doi.org/10.1016/0378-1119(93)90551-D.
81. Studier, F.W. (2005). Protein production by auto-induction in high density shaking cultures. Protein Expr. Purif. *41*, 207–234. https://doi.org/10.1016/j.pep.2005.01.016.
82. Rappsilber, J., Mann, M., and Ishihama, Y. (2007). Protocol for micro-purification, enrichment, pre-fractionation and storage of peptides for proteomics using StageTips. Nat. Protoc. *2*, 1896–1906. https://doi.org/10.1038/nprot.2007.261.
83. Olsen, J.V., Macek, B., Lange, O., Makarov, A., Horning, S., and Mann, M. (2007). Higher-energy C-trap dissociation for peptide modification analysis. Nat. Methods *4*, 709–712. https://doi.org/10.1038/nmeth1060.
84. Cox, J., Neuhauser, N., Michalski, A., Scheltema, R.A., Olsen, J.V., and Mann, M. (2011). Andromeda: a peptide search engine integrated into the MaxQuant environment. J. Proteome Res. *10*, 1794–1805. https://doi.org/10.1021/pr101065j.
85. Cox, J., Hein, M.Y., Luber, C.A., Paron, I., Nagaraj, N., and Mann, M. (2014). Accurate proteome-wide label-free quantification by delayed normalization and maximal peptide ratio extraction, termed MaxLFQ. Mol. Cell. Proteomics *13*, 2513–2526. https://doi.org/10.1074/mcp.M113.031591.
86. Schwanhäusser, B., Busse, D., Li, N., Dittmar, G., Schuchhardt, J., Wolf, J., Chen, W., and Selbach, M. (2011). Global quantification of mammalian gene expression control. Nature *473*, 337–342. https://doi.org/10.1038/nature10098.

STAR★METHODS

KEY RESOURCES TABLE

REAGENT or RESOURCE	SOURCE	IDENTIFIER
Antibodies		
Donkey anti-mouse Alexa-488	ThermoFisher	RRID: AB_2534082
Donkey anti-sheep Alexa-594	ThermoFisher	RRID: AB_2534083
Mouse anti-Flag (M2)	Sigma	Cat #F1804-5MG; RRID: AB_262044
Mouse anti-GFP	ThermoFisher	Cat #A11122; RRID: AB_221569
Mouse anti-GFP (JL-8)	Living Colors	Cat #632380; RRID: AB_10013427
Mouse anti-myc (9E10)	Covance	Cat #MMS-150P-1000; RRID: AB_291322
Mouse anti-V5	Bio-Rad	Cat #MCA1360; RRID: AB_322378
Sheep anti-Cdc11	Gift from Ken Sawin	N/A
Tat1 (anti-tubulin)	Gift from Ian Hagan	N/A
Bacterial and virus strains		
BL21-CodonPlus (DE3)-RIPL *E. coli*	Stratagene	Cat #230280
NEB 5-alpha Competent *E. coli* (High Efficiency)	New England Biolabs	Cat #C2987H
Chemicals, peptides, and recombinant proteins		
Benzonase	EMD Millipore	CAS #9025-65-4
Chelex	BioRad	Cat #1421253
Dimethyl pimelimidate	ThermoFisher	Cat #21666
Formaldehyde, 37%	MERCK	CAS #F8775
Protein G Dynabeads	ThermoFisher	Cat #10009D
Protein G-Agarose	Roche	Cat #11243233001
RapiGest SF	Waters	Cat #186001860
Trypsin	Pierce	Cat #90057
Zymolyase-100T	MP Biomedicals	Cat #08320932
Critical commercial assays		
FastStart Taq DNA Polymerase	Roche	Cat #12032953001
Imperial Protein Stain	ThermoFisher	Cat #24615
Light Cycler 480 SybrGreen Master Mix	Roche	Cat #04887352001
Monarch Plasmid Miniprep Kit	New England Biolabs	Cat #T1010L
NEB Golden Gate Assembly Kit (BsaI-HF v2)	New England Biolabs	Cat #E1601S
QIAquick PCR Purification Kit	QIAGEN	Cat #28104
Silverquest™ Silver Staining Kit	ThermoFisher	Cat #LC6070
Experimental models: Organisms/strains		
S. pombe strains, see Table S2	This study	N/A
Oligonucleotides		
Primers, see Table S3	This study	N/A
Recombinant DNAs		
Plasmids, see Table S4	This study	N/A
Software and algorithms		
Fiji	http://fiji.sc	RRID: SCR_002285
Imagelab Touch v 3.0.1.14	BioRad	N/A
Maxquant v. 1.6.1.0	Cox and Mann[76]	RRID: SCR_014485
Nikon NIS Elements software v. 5.2	Nikon	RRID: SCR_014329
Perseus v. 1.6.2.1	Tyanova et al.[77]	RRID: SCR_015753
Prism Version 9.5	Graphpad	RRID: SCR_002798
Roche LightCycler software version 1.5.1.62	Roche	N/A

(*Continued on next page*)

Continued

REAGENT or RESOURCE	SOURCE	IDENTIFIER
SnapGene 5.2.5	GSL Biotech LLC	RRID: SCR_015052
Other		
Amicon 10k MWCO filters	Millipore	Cat #UFC901024
Amylose resin	NEB	Cat #E8021S
C_{18} reverse-phase resin	Sigma	Cat #66883-U
HisPur™ Ni-NTA resin	ThermoFisher	Cat #88222
HiTrap™ HP	Cytiva	Cat #17-5248-02
Poly-lysine-coated slides	Epredia	Cat #J2800AMNZ
TALON resin	Takara	Cat #635502
Vectashield mounting medium	Vector Laboratories	Cat #H-1000
Vectashield mounting medium with DAPI	Vector Laboratories	Cat #H-1200
Vivacon 30k MWCO spin filter	Sartorius	Cat #VN01H21

RESOURCE AVAILABILITY

Lead contact

Requests concerning resources or material should be directed to and will be fulfilled by the lead contact Robin Allshire (robin.allshire@ed.ac.uk).

Materials availability

All plasmids and *S. pombe* strains generated or used for this study are available form the lead contact without restriction

Data and code availability

- All data reported in this paper will be shared by the lead contact upon request.
- This paper does not report original code.
- Any additional information required to reanalyze the data reported in this paper is available from the lead contact upon request.

EXPERIMENTAL MODEL AND SUBJECT DETAILS

Yeast strain construction

S. pombe strains used in this study are listed in Table S2. C-terminal taggings and deletions were performed on genes at the endogenous locus using standard homologous recombination-based methods.[78] Candidate transformants were verified by genomic PCR, microscopy, western blotting, or phenotypic analysis as appropriate. CRISPR/Cas9 was used to insert TEV sites, to N-terminally tag *sad1*, and to generate the *sad1-1* mutation (A323V) at the endogenous *sad1* locus. Cells were co-transformed with the guide RNA plasmid and homologous recombination templates generated by primer annealing, followed by selection and screening.[79] Sad1 N-terminal tagging, TEV-site insertion, and 4A mutations were confirmed by genomic DNA amplification and sequencing with NL266-NL284, and *sad1-1* was similarly verified with NL265-267. *mis18Δ169-194* and *cnp3Δ325-490* were generated by CRISPR-Cas9 and PCR-based verification with NL142-NL360 and NL386-NL387, respectively.

NLS-9myc-TEV-2xNLS and ectopic *sad1* alleles were integrated at the *ars1* locus by transforming MluI-digested pNL142 (TEV), BlpI-digested pNL190 (*psad1-sad1*), or BlpI-digested pNL197 (*psad1-sad1-4A*). Transformants were passaged without selection to single colonies for multiple generations to reduce the likelihood of retaining any episomal DNA and were subsequently crossed to generate the experimental strains. *TEV* and ectopic *sad1* integration were verified by PCR with NL362-NL363. *csi1*Δ was obtained from the Bioneer Deletion Set V1-17E7.

Yeast growth conditions

TEV expression was induced by thiamine washout. Starter cultures were grown in YES (Yeast Extract with Supplements) media, then washed in PMG (*Pombe* Minimal Glutamate) media without thiamine and used to inoculate sample cultures in PMG supplemented with amino acids and with or without 15 μM thiamine. These cells were grown for 10 hours, or the indicated time, at 32°C. 4x concentrated YES media was used for MS experiments not involving TEV expression. For other experiments, cells were cultured at 32°C in YES. For temperature shifts, starter cultures were grown at 25°C then diluted to appropriate densities and grown at 25°C or 36°C for 8 hrs. In all cases, cells were cultured to approximate densities of OD_{600} = 0.5-1.0 for microscopy and qChIP experiments or 1.0-2.0

for IP/MS experiments. For growth assays, 1:5 serial dilutions were plated and grown for 3-5 days under the indicated conditions until colonies were fully developed. Phloxine B was used at 2.5 μg/mL.

METHOD DETAILS

Cloning

DNA primers used are listed in Table S3 and plasmids are listed in Table S4. The TEV-protease expression plasmid was generated by PCR amplifying NLS-9myc-TEV-2xNLS from AMp1325 with NL332-NL333 and inserting into BamHI/SalI-digested pRep1 downstream of the thiamine-repressible *nmt1* promoter[80] via Gibson assembly. CRISPR/Cas9 targeting constructs were generated by Golden Gate assembly (NEB cat #E1601S) using pLSB plasmids as described.[79] Briefly, target sequence primers were annealed and incubated with the destination vector in the presence of Golden Gate assembly mix at 37°C for 1 hr, then 60°C for 5 min before transformation into *E. coli*. The ectopic *sad1* integration construct (pNL190) was generated by PCR amplifying the *sad1* ORF from genomic *S. pombe* DNA with NL456-NL457, annealing NL458-NL459 to generate the 3Flag sequence, and Gibson assembling these fragments with BamHI-HF/SphI-digested vector (derived from pRad11, a gift from Y. Watanabe). PCR-based mutagenesis of pNL190 was performed with NL453-NL467 to generate the ectopic *sad1-4A* construct (pNL197).

Mis18 codon optimized sequences (GeneArt) were cloned into pET His6 msfGFP TEV (9GFP) cloning vector with BioBrick polycistronic restriction sites or into pEC-K-3C-His (a kind gift from Elena Conti). *Sad1*$_{2\text{-}167}$ was amplified with NL389-NL390 and ligated into pET-6His-TEV (9B) or pET-6His-MBP-TEV (9C) with ligation-independent cloning (LIC) to generate 6His-TEV-Sad1$_{2\text{-}167}$ or 6His-MBP-Sad1$_{2\text{-}167}$ plasmids, respectively. For the 6His-Sad1$_{2\text{-}167}$ 6His-Mis18$_{FL}$ coexpression plasmid, Sad1$_{2\text{-}167}$ sequence was excised from pNL188 with NcoI/PacI digestion and ligated with NotI/AsiSI-digested 6His-Mis18 vector. 6HIS-GFP was generated by amplifying GFP with NL461-NL462 and ligating into 9B by LIC. 9B, 9C, and 9GFP were gifts from Scott Gradia. (9B: Addgene plasmid # 48284; http://n2t.net/addgene:48284; RRID: Addgene_48284; 9C: Addgene plasmid # 48286; http://n2t.net/addgene:48286; RRID: Addgene_48286; 9GFP: Addgene plasmid # 48287; http://n2t.net/addgene:48287; RRID: Addgene_48287)

Protein expression

Analysis of sad1-TEV protein cleavage, TEV protease expression, sad1-4A protein levels, and ectopic Sad1 protein levels were performed by lysing cells in Laemmli sample buffer (2% SDS, 10% glycerol, 62.5 mM Tris-HCl pH 6.8, 0.002% bromphenol blue) with 2 mM PMSF and 1 mM DTT by bead beating. Samples were heated to 95°C for 3 min, pelleted at 13.2k RPM in a 4°C microfuge for 5 min, and analyzed by western blotting. α-V5 (Bio-Rad cat #MCA1360) was used at 1:5,000, α-GFP (JL-8, Living Colors cat #632380) was used at 1:1,000, α-Flag (Sigma cat #F1804-5MG) was used at 1:1,000, α-myc (9E10) was used at 1:5,000, and Tat1 (α-tubulin, from Iain Hagan) was used at 1:10,000.

Protein purification and size exclusion chromatography

6His-Sad1$_{2\text{-}167}$, 6His-MBP-Sad1$_{2\text{-}167}$, 6His-Mis18, 6His-GFP, and 6His-MBP expression plasmids were transformed into BL21-CodonPlus (DE3)-RIPL *E. coli* (Stratagene, #230280) and recovered on non-inducing MDAG media[81] with carbenicillin, streptomycin, and chloramphenicol selection. Transformed cells were grown in 2xYT (1.6% tryptone, 1.0% yeast extract, 0.5% NaCl at pH 7.0) with carbenicillin and streptomycin to mid-log phase (O.D.$_{600}$ of 0.5-1.0) at 36°C, then induced with 0.1 mM IPTG and cultured at 18°C for 16 hrs. Cells were then pelleted and flash frozen. Cells were resuspended in lysis buffer (20 mM HEPES pH 7.0, 500 mM NaCl, 5% glycerol, 2 mM dithiothreitol (DTT), 1 mM phenylmethylsulfonyl fluoride (PMSF)) and lysed by sonication. Lysate was pelleted at 15,000 x g for 30 min at 4°C. Supernatant was incubated with 1 column volume (CV) of TALON resin (Takara #635502) at 4°C for 1-2 hours. Resin was washed in 20 CV wash buffer (lysis buffer + 5 mM imidazole), then eluted in 0.5-1 mL fractions with elution buffer (20 mM HEPES pH 7.0, 300 mM NaCl, 5% glycerol, 150 mM imidazole, 2 mM DTT). For size exclusion chromatography (SEC) of 6His-Sad1$_{2\text{-}167}$ and 6His-Mis18, proteins were concentrated using Amicon 10k MWCO filters (Millipore #UFC901024). SEC was performed with a Superdex 200 10/300 GL column on an ÄKTA Pure™ 25 (Cytiva) system and a buffer consisting of 20 mM HEPES pH 7.0, 150 mM NaCl, and 2 mM DTT.

All other Mis18 constructs were expressed in BL21 Gold cells. 6His-msfGFP-TEV-Mis18$_{121\text{-}194}$ and 6His-msfGFP-TEV-Mis18$_{FL}$ were grown in 2xYT while 6His-3C-Mis18$_{1\text{-}120}$ and 6His-3C-Mis18$_{1\text{-}168}$ were grown in Super Broth. For Mis18$_{FL}$, Mis18$_{121\text{-}194}$ and Mis18$_{1\text{-}168}$, after entering log phase (O.D.$_{600}$ = 0.6-0.8) the temperature was reduce to 18°C for one hour and IPTG was added to final concentration of 0.3 mM and protein was induced overnight. For Mis18$_{1\text{-}120}$, induction occurred at 25°C for 6 hours.

6His-Mis18$_{1\text{-}168}$ was lysed in lysis buffer containing 20 mM Tris (pH8.0 at 4°C), 50 mM NaCl, 35 mM imidazole and 2 mM β-mercaptoethanol (βME) and supplemented with DNase (Sigma #DN25-100mg) to a concentration of 10 μg/mL and cOmplete™ EDTA-free protease inhibitors (Sigma #05056489001), 1 tab per 50 mL. Cells were lysed by sonication and centrifuged at 22,000 rpm for 50 mins at 4°C. Clarified lysates were incubated with HisPur™ Ni-NTA resin (Thermo Fisher #88222) and washed extensively with 100 CV of lysis buffer before elution with lysis buffer containing 500 mM imidazole. The protein was concentrated and SEC was performed on an ÄKTA system (Cytiva) using a S200 Hiload 16/600 column (Cytiva) equilibrated with 20 mM Tris (pH8.0 at 4°C), 50 mM NaCl, and 4 mM DTT.

6His-Mis18$_{1\text{-}120}$ was lysed in lysis buffer containing 20 mM Tris (pH 8.0 at 4°C), 500 mM NaCl, 35 mM imidazole and 5 mM βME and supplemented with DNase to a concentration of 10 μg/mL and cOmplete™ EDTA free protease inhibitors, 1 tab per 50 mL. Cells were lysed by sonication and centrifuged at 22,000 rpm for 50 mins at 4°C. Clarified lysates were incubated with 5ml HisTrap™ HP (Cytiva

#17-5248-02) and washed with 40 CV lysis buffer, then 35 CV of a high salt buffer containing 20 mM Tris (pH 8.0 at 4°C), 1 M NaCl, 35 mM imidazole, 10 mM MgCl, 50 mM KCl, 2 mM ATP and 5 mM βME, then 20 CV of lysis buffer before elution with lysis buffer containing 500 mM imidazole.

6His-GFP-Mis18$_{FL}$ and 6His-GFP-Mis18$_{121-194}$ were lysed in lysis buffer containing 20 mM Tris (pH 8.0 at 4°C), 100 mM NaCl, 35 mM imidazole and 5 mM βME and supplemented with DNase to a concentration of 10 μg/mL and cOmplete™ EDTA free protease inhibitors, 1 tab per 50 mL. Cells were lysed by sonication and centrifuged at 22,000 rpm for 50 mins at 4°C. Clarified lysates were incubated with 5ml HisTrap™ HP and washed with 40 CV of lysis buffer, then 35 CV of high salt buffer containing 20 mM Tris (pH 8.0 at 4°C), 1 M NaCl, 35 mM imidazole, 10 mM MgCl, 50 mM KCl, 2 mM ATP and 5 mM βME, then 20 CV of lysis buffer before elution with a lysis buffer containing 500 mM imidazole. The proteins were concentrated and SEC was performed on an ÄKTA system using a S200 increase 10/300 column (Cytiva) equilibrated with 20 mM Tris (pH 8.0 at 4°C), 150 mM NaCl, and 2 mM DTT.

Protein binding assays

Amylose resin (NEB cat #E8021S) was washed with binding buffer (20 mM HEPES pH 7.0, 150 mM NaCl, 1 mM TCEP, 0.01% Tween-20). 6His-MBP or 6His-MBP-Sad1$_{2-167}$ were mixed with candidate binding proteins and resin with each protein at 5 μM. "Total" samples were taken, and reactions were incubated at 4°C for 1 hr with gentle rotation. Resin was then pelleted and washed in 4 exchanges of 500 μL binding buffer. All supernatant was removed, sample buffer was added, and samples were boiled at 95°C for 3 minutes to yield the "Pulldown" sample. Equivalent proportions of the total reaction from "Total" and "Pulldown" samples were loaded on SDS-PAGE gels (NuPage, cat #NP0322BOX), which were stained with Imperial Protein Stain (Coomassie R-250, ThermoFisher, cat #24615).

qChIP

For endogenous centromere CENP-A ChIP assays, replicate cultures were grown in YES media (3+ cultures of the same genotype). *sad1-1*-containing strain starter cultures were grown at 25°C to log phase and used to inoculate sample cultures at 25°C or at 36°C for 8 hrs before fixation. For Sad1-TEV140-3V5 ChIP, starter replicate cultures were grown in YES, then washed in media without thiamine, and used to inoculate PMG complete media with or without 15 μM thiamine and cultured for 10 hrs at 32°C. Efficient Sad1-TEV140-3V5 cleavage was assayed by western. For CENP-A establishment assays, fresh pHcc2 transformants were cultured in PMG -adenine-uracil media to log phase. Before fixation, a sample of cells was plated on selective media, then replica -plated to YES low adenine media (10 μg/mL adenine) to test for red/white colony sectoring. Pure white colonies on low adenine indicates plasmid integration, so samples harvested from strains with a high proportion (>10%) of pure white colonies were omitted from further processing. In all cases, cells were fixed at approximately OD_{600} = 1.0 by addition of formaldehyde (Merck, CAS# 50-00-0) to 1% followed by 15 min incubation at RT. Crosslinking was quenched with 125 mM glycine for 5 min. Cells were pelleted, washed in phosphate buffered saline (PBS), and snap frozen in liquid nitrogen before being processed for qPCR analysis.

Immunoprecipitation

For coIP and MS experiments, cells were grown to log phase (approximate OD_{600} = 2.0) in YES or 4xYES, pelleted, resuspended in SPB lysis buffer with protease inhibtors and phosphatase inhibitors, and flash frozen as pellets. SPB lysis buffer was 25 mM HEPES, 150 mM KCl, 2 mM MgCl2, 0.5% Triton-X 100, 10% glycerol, and was supplemented with 1 mM DTT. Protease inhibitors were 1 mM PMSF and a cocktail (Sigma, cat #P-8215) used at 1:100 dilution. Phosphatase inhibitors were 10 ng/mL microcystin (Enzo cat #ALX350-012-C100), 1 mM sodium pyrophosphate, 100 μM sodium orthovanadate, 5 mM sodium fluoride, and 2 mM β-glycerophosphate. For Figures 1 and S1 experiments, lysis was performed with a Retsch MM400 ball mill with 3 rounds of milling at 30 cycles/second for 2 min/cycle with 2 min in liquid nitrogen between rounds. For other MS and IP experiments, cryo-lysis was performed with a freezer mill (Spex 6875) with 8-10 rounds of 2" at 10 cycles /second. Lysate was gently sonicated, treated with 50 u/mL benzonase (EMD Millipore, Cas #9025-65-4) at 4°C for 1 hr, then pelleted at 4,700 g for 10 min at 4°C. α-V5 or α-Flag M2 antibodies were conjugated to Protein G Dynabeads (ThermoFisher cat #10009D) by crosslinking with dimethyl pimelimidate (DMP, ThermoFisher cat #21666). Beads were incubated with lysate supernatant at 4° for 2 hrs, then washed with 5 exchanges of SPB lysis buffer, including 1 mM DTT, 0.2 mM PMSF, 1:500 protease inhibitors, and phosphatase inhibitors in the first three washes. For coIP, beads were eluted in Laemmli sample buffer by heating to 95°C for 3 minutes, then transferring supernatant to a new tube and treating with reducing 50 mM DTT. For MS, beads were eluted in 2 sequential rounds with 0.1% RapiGest SF (Waters cat #186001860) in 50mM Tris-HCl pH 8 by incubating at 50°C for 10 minutes with mixing. Eluate from the second round was pooled with that of the first round for analysis and further processing. Samples were analyzed by SDS-PAGE electrophoresis and silver staining (ThermoFisher cat #LC6070) or western blotting.

Mass spectrometry

IP eluate was reduced with 25 mM DTT at 80°C for 1 min, then denatured by addition of urea to 8M. Sample was applied to a Vivacon 30k MWCO spin filter (Sartorius cat #VN01H21) and centrifuged at 12.5k g for 15-20 minutes. Protein retained on the column was then alkylated with 100 μL of 50 μM iodoacetamide (IAA) in buffer A (8 M urea, 100 mM Tris pH 8.0) in the dark at RT for 20 min. The column was then centrifuged as before, and washed with 100 μL buffer A, then with 2 x 100 μL volumes of 50 mM ammonium bicarbonate (AmBic). 3 μg/μL trypsin (Pierce #90057) in 0.5 mM AmBic was applied to the column, which was capped and incubated at 37°C overnight. Digested peptides were then spun through the filter, acidified with trifluoroacetic acid (TFA) to pH <= 2, loaded onto

manually-prepared and equilibrated C_{18} reverse-phase resin stage tips (Sigma #66883-U),[82] washed with 100 uL 0.1% TFA, and stored at -20°C prior to MS analysis.

Peptides were eluted in 40 μL of 80% acetonitrile in 0.1% TFA and concentrated down to 2 μL by vacuum centrifugation (Concentrator 5301, Eppendorf, UK). The peptide sample was then prepared for LC-MS/MS analysis by diluting it to 5 μL by 0.1% TFA. LC-MS-analyses were performed on an Orbitrap Fusion™ Lumos™ Tribrid™ Mass Spectrometer (Thermo Scientific, UK) coupled on-line to an Ultimate 3000 RSLCnano Systems (Dionex, Thermo Fisher Scientific, UK). In both cases, peptides were separated on a 50 cm EASY-Spray column (Thermo Scientific, UK), which was assembled on an EASY-Spray source (Thermo Scientific, UK) and operated at 50°C. Mobile phase A consisted of 0.1% formic acid in LC-MS grade water and mobile phase B consisted of 80% acetonitrile and 0.1% formic acid. Peptides were loaded onto the column at a flow rate of 0.3 μL per min and eluted at a flow rate of 0.25 μL per min according to the following gradient: 2 to 40% mobile phase B in 150 min and then to 95% in 11 min. Mobile phase B was retained at 95% for 5 min and returned back to 2% a minute after until the end of the run (190 min). FTMS spectra were recorded at 120,000 resolution (scan range 350-1500 m/z) with an ion target of 7.0×10^5. MS2 was performed in the ion trap with ion target of 1.0×10^4 and HCD fragmentation[83] with normalized collision energy of 27. The isolation window in the quadrupole was 1.4 Thomson. Only ions with charge between 2 and 7 were selected for MS2. The MaxQuant software platform[76] version 1.6.1.0 was used to process the raw files and search was conducted against *Schizosaccharomyces pombe* complete/reference proteome set of PomBase database (released in July, 2016), using the Andromeda search engine.[84] For the first search, peptide tolerance was set to 20 ppm while for the main search peptide tolerance was set to 4.5 pm. Isotope mass tolerance was 2 ppm and maximum charge to 7. Digestion mode was set to specific with trypsin allowing maximum of two missed cleavages. Carbamidomethylation of cysteine was set as fixed modification. Oxidation of methionine was set as variable modification. Label-free quantitation analysis was performed by employing the MaxLFQ algorithm as described.[85] Absolute protein quantification was performed as described.[86] Peptide and protein identifications were filtered to 1% FDR.

Perseus[77] version 1.6.2.1 was used to analyze output of the MaxQuant searches. Protein identifications based on reverse peptide, potential contaminant, and "only-site" IDs (only modified peptides) were filtered out, as were IDs with less than 2 valid peptide IDs. Intensity values were Log_2 transformed to facilitate statistical analysis. Data from 3 replicate cultures for each genotype or condition were grouped, and proteins with less than 2 valid values in at least one group were filtered out. Imputation replaced missing values from a normal distribution with settings width = 0.3 and downshift = 1.8. Volcano plots were generated using 2-sample Student's t-tests with a p-value of 0.05 (alpha = 0.05). Horizontal cutoffs at y = 1.3 on the plots represent statistical significance by this test. Vertical lines were drawn at Log_2(+/-2) enrichment as a guide for meaningful abundance differences. All mass spectrometry proteomics data have been deposited to the ProteomeXchange Consortium via the PRIDE partner repository with the dataset identifier PXD045191

qChIP

3 or more biological replicates of approximately 2.5×10^8 cells of were prepared of each ChIP sample. Cells were lysed by bead beating in 350 μL ChIP lysis buffer (50 mM HEPES-KOH, pH 7.5, 140 mM NaCl, 1 mM EDTA, 1% (v/v) Triton X-100, 0.1% (w/v) sodium deoxycholate), then sonicated to solubilize chromatin (20 cycles of 30 sec on + 30 sec off in a 4°C water bath Diagenode Bioruptor on "high"). Cellular debris was removed by centrifugation at 13.2k rpm for 10 min at 4°C. For α-Cnp1 ChIP, lysate was pre-cleared by incubating with Protein G agarose resin (Roche, CAS #64-17-5) at 4°C for 1 hr. Resin was then removed, input sample was taken, and the remaining supernatant was incubated with Protein G resin plus α-Cnp1 (in house serum, used at 4 uL and 25 uL resin per ChIP). For α-V5 and α-GFP ChIP, the preclearing step was omitted and 25 uL of Protein G Dynabeads were used with 3 μL of α-V5 or 2 μL of α-GFP (ThermoFisher, cat #A11122). IP's were performed overnight at 4°C. Resin or beads were washed with ChIP Lysis Buffer, then the same buffer with 0.5M NaCl, then ChIP Wash Buffer (10 mM Tris-HCl, pH8, 0.25 M LiCl, 0.5% NP-40, 0.5% (w/v) sodium deoxycholate, 1 mM EDTA), then TE (10 mM Tris-HCl, pH8, 1 mM EDTA), and then processed in tandem with input samples. All samples were incubated with a 10% slurry of Chelex 100 (BioRad cat #1421253) at 100°C for 12 min to reverse crosslinks, then cooled to room temperature and incubated at 55°C with 25 μg of Proteinase K for 30 min. Samples were heated to 100°C for 10 min to inactivate Proteinase K. Resin was pelleted and supernatant was collected for ChIP reactions. qPCR was performed in triplicate for each sample using primers specific for *actin* or centromeric sequence (see Table S3) using LightCycler 480 SYBR Green I Master mix (Roche, 04887352001) on a Roche LightCycler 480 Instrument and LightCycler 480 software v. 1.5.1.62. Analysis is described in "quantitation and statistical analysis" section.

Immunofluorescence

Cells were fixed in 3.7% formaldehyde for 15 min at RT, then washed 2x in PEM (100 mM PIPES, pH 7.0, 1 mM EDTA, 1 mM $MgCl_2$), 1x in PEMS (PEM + 1.2 M sorbitol), and stored in PEM + 0.1% sodium azide at 4°C. Fixed cells were treated with 1 mg/mL zymolyase T100 (MP Biomedicals cat #08320932) at 37°C for 90 min, washed in PEMS, then permeabilized in PEMS + 1% Triton-X100 for 1 min. Next, cells were washed in PEMS, then 2x in PEM, then blocked for 30 min in PEMBAL (PEM + 1% Bovine Serum Albumin (BSA), 100 mM lysine hydrochloride, 0.1 sodium azide). Cells were incubated with primary mouse α-V5 and sheep α-Cdc11 at 1:1,000 in PEMBAL at 4°C overnight. 3 x 30 minute washes in PEMBAL were followed by secondary donkey α-mouse Alexa-488 (ThermoFisher RRID: AB_2534082) and donkey α-sheep Alexa-594 (ThermoFisher RRID: AB_2534083) incubation, both at 1:1,000 (2 μg/mL) in PEM, at 4°C for 4 hrs in the dark. Following a PEMBAL wash, cells were stained with 2 μg/mL 4',6-diamidino-2-phenylindole (DAPI) in PEM at RT for 5 min. Finally, cells were washed once and stored in PEM + 0.1% azide at 4°C.

Microscopy and image analysis

Fixation was performed by adding formaldehyde to 3.7% and incubating at room temperature for 15 minutes. Cells were washed twice in PEM, then 1x in PEMS. Cells were then stored in PEM + 0.01% sodium azide at 4°C. For imaging, fixed cells were mounted on poly-lysine-coated glass slides (Epredia cat #J2800AMNZ) with Vectashield mounting medium (Vector Laboratories cat #H-1200) containing 1.5 μg/mL 4',6-diamidino-2-phenylindole (DAPI). For IF samples, mounting media without DAPI was used (Vector Laboratories cat #H-1000).

Images were acquired on a Nikon Eclipse Ti2 inverted microscope with a Lumencore Spectra X lightsource (Beaverton, OR, USA) and a Photometrics Prime 95B camera (Teledyne Photometrics, Birmingham, UK) controlled with Nikon Elements v. 5.2. The stage was controlled with a MadCity Nanodrive (Mad City Labs, Madison, WI, USA). Images were acquired using a 100x 1.49 NA CFI Plan Apochromat TIRF objective. Semrock filter sets were used (excitation 378 nm/emission 460 nm; excitation 488 nm/emission 535 nm; and excitation 578 nm/emission 630 nm). Z-stacks of each field were taken at 0.2 uM steps for 11 slices.

To quantify Csi1-GFP and Lem2-GFP intensity, images were max projected in FIJI. Circular 7x7 pixel regions encompassing individual Sid4-mCherry foci were designated as regions of interest (ROIs), and intensity measurements were made in both red and green channels. A background (cell free region) intensity measurement of the same dimensions was subtracted from ROI intensity measurements in both channels. The adjusted green signal channel intensity was divided by the adjusted red signal channel intensity for each ROI to yield a normalized GFP intensity measurement.

QUANTIFICATION AND STATISTICAL ANALYSIS

qPCR results were quantified with LightCycler 480 software v. 1.5.1.62 and analyzed with Graphpad Prism v. 9.5 (RRID: SCR_002798). Ct values of triplicate PCRs from each biological replicate were averaged and percent IP was calculated as the ratio of the "IP" sample Ct value to the "Input" Ct value. Where indicated, percent IP of the target locus was normalized to percent IP of the *actin* locus. Comparisons between biological replicates were performed using Welch's t-test and bar graphs show means, standard deviations, and individual data points (n = 3-11 biological replicates) as described in the figure legends.

For microscopy experiments, the number of cells analyzed (n) is given in the figure for each condition. Data was analyzed by χ^2 test using Graphpad Prism v 9.5.

Statistical analysis of mass spectrometry data is described in the "mass spectrometry" section.

To quantify Sad1-TEV140-3V5 cleavage, digital exposures were taken of westerns using a BioRad ChemiDoc MP running ImageLab Touch v. 3.0.1.14. Rectangular boxes covering the area of the bands of interest were selected and total intensity was measured in ImageJ. Equivalent background measurements were subtracted from these measurements. The resulting intensities of the cleaved band were divided by the corresponding intensities of the cleaved plus uncleaved bands to yield the proportion cleaved.